

Characterization of conventional kinesins Kif3 and Kif5 from *Dictyostelium discoideum*

Dissertation
der Fakultät für Biologie der
Ludwig-Maximilians-Universität
München

vorgelegt von
Christian Röhlk
aus Göttingen
Juni 2007

Ehrenwörtliche Versicherung

Hiermit versichere ich, dass ich die vorliegende Arbeit selbständig und ohne unerlaubte Hilfsmittel angefertigt habe.

Christian Röhlk

München, Juni 2007

Dissertation eingereicht: 28.06.2007

Tag der mündlichen Prüfung: 27.07.2007

Mentor (Erstgutachter): PD Dr. Günther Woehlke

Zweitgutachter: Prof. Dr. Charles David

Parts of this work have been published:

Christian Roehlk, Sven Leier, Manfred Schliwa, Xiao Liu, John Parsch, Guenther Woehlke (2007)

Properties of the Kinesin-1 Motor Kif3 from *Dictyostelium discoideum*

Eur. J. Cell Biol. submitted on June 11, 2007

Meeting abstracts:

Christian Roehlk, Guenther Woehlke

Characterizing Kinesin3 and DdKin5 from *Dictyostelium discoideum*

46th annual meeting of the American Society for Cell Biology; Dec 9-13, 2006, San Diego, CA, USA

The work presented here was carried out in the laboratory of Prof. Dr. Manfred Schliwa (Institute for Cell Biology of the Ludwig-Maximilians-University, Munich) from October 2003 till May 2007.

Contents

SUMMARY	IV
ABBREVIATIONS	V
1 INTRODUCTION	1
1.1 CYTOSKELETON AND CELLULAR MOTILITY	1
1.1.1 <i>Microtubules</i>	1
1.1.2 <i>Motor proteins</i>	1
1.2 <i>DICTYOSTELIUM DISCOIDEUM</i>	5
1.3 KINESINS IN <i>DICTYOSTELIUM</i>	6
1.3.1 <i>Kif3 (Kinesin-1 subfamily)</i>	8
1.3.2 <i>Kif5 (Kinesin-1 subfamily)</i>	8
1.4 AIMS OF THE WORK	8
2 MATERIALS & METHODS	9
2.1 MATERIALS	9
2.1.1 <i>Reagents and other materials</i>	9
2.1.2 <i>Vectors</i>	9
2.1.3 <i>Antibodies</i>	9
2.1.4 <i>Other markers</i>	10
2.2 ORGANISMS	10
2.2.1 <i>D. discoideum strains</i>	10
2.2.2 <i>Media and cultivation of D. discoideum</i>	10
2.2.3 <i>Bacterial strains</i>	11
2.2.4 <i>Media and cultivation of E. coli</i>	11
2.3 MOLECULAR BIOLOGY METHODS	12
2.3.1 <i>Agarose gel electrophoresis</i>	12
2.3.2 <i>DNA extraction from agarose gels</i>	12
2.3.3 <i>Determination of DNA concentrations</i>	12
2.3.4 <i>Preparation of plasmid DNA</i>	12
2.3.5 <i>Preparation of chromosomal DNA</i>	12
2.3.6 <i>Isolation of polyadenylated RNA</i>	13
2.3.7 <i>Polymerase chain reaction (PCR)</i>	13
2.3.8 <i>Reverse transcription PCR (RT-PCR)</i>	13
2.3.9 <i>DNA cleavage with restriction enzymes</i>	14
2.3.10 <i>Site directed mutagenesis</i>	14

2.3.11	<i>Ligation</i>	14
2.3.12	<i>Preparation and transformation of competent cells</i>	14
2.3.13	<i>Colony check PCR</i>	15
2.3.14	<i>Construction of null-mutants</i>	16
2.3.15	<i>Generation of expression constructs</i>	16
2.3.16	<i>Transformation of Dictyostelium cells</i>	18
2.3.17	<i>Southern blotting</i>	19
2.3.18	<i>DiG hybridization</i>	19
2.4	BIOCHEMICAL METHODS	20
2.4.1	<i>SDS-polyacrylamide gel electrophoresis</i>	20
2.4.2	<i>Staining of SDS-gels</i>	21
2.4.3	<i>Expression of kinesin constructs</i>	21
2.4.4	<i>Protein purification</i>	21
2.4.5	<i>Purification of pig brain tubulin</i>	23
2.4.6	<i>Determination of protein concentration</i>	25
2.4.7	<i>Polymerization of microtubules</i>	25
2.4.8	<i>Microtubule-stimulated ATPase activity</i>	25
2.4.9	<i>Multiple motor gliding assay</i>	27
2.4.10	<i>Gliding of kinesin labeled with quantum dots</i>	27
2.4.11	<i>Purification of the Kif3-342 antibody</i>	28
2.4.12	<i>Western blots and immunostaining</i>	28
2.4.13	<i>Determination of oligomerization state</i>	29
2.4.14	<i>Isolation of mitochondria from Dictyostelium cells</i>	30
2.4.15	<i>Immunoprecipitation</i>	31
2.5	CELL BIOLOGICAL METHODS	31
2.5.1	<i>Immunofluorescence microscopy</i>	31
2.5.2	<i>Microtubule reorganization experiment</i>	32
2.5.3	<i>Phylogenetic analysis</i>	33
3	RESULTS	34
3.1	<i>D. DISCOIDEUM KINESIN KIF3</i>	34
3.1.1	<i>Phylogenetic analysis</i>	34
3.1.2	<i>Kif3-null mutants</i>	35
3.1.3	<i>Expression and purification of Kif3 constructs</i>	36
3.1.4	<i>Oligomerization states</i>	36
3.1.5	<i>Microtubule-stimulated ATPase activity</i>	37
3.1.6	<i>Motility</i>	40
3.1.7	<i>Duty ratio of Kif3-constructs</i>	41
3.1.8	<i>Summary of Kif3's biochemical properties</i>	41
3.1.9	<i>Kif3 GFP-fusion proteins and immunofluorescence</i>	41
3.1.10	<i>Western Blots</i>	45

Contents	III
3.1.11 Immunoprecipitation	46
3.2 <i>D. DISCOIDEUM</i> KINESIN KIF5	47
3.2.1 <i>Kif5</i> -null mutants	47
3.2.2 Expression and purification of <i>Kif5</i> constructs	49
3.2.3 Microtubule-stimulated ATPase activity	50
3.2.4 Motility	50
3.2.5 <i>Kif5</i> GFP-fusion protein	51
4 DISCUSSION	52
4.1 <i>D. DISCOIDEUM</i> KIF3	52
4.1.1 Biochemical <i>in vitro</i> properties	52
4.1.2 Cellular localization and function of <i>Kif3</i>	54
4.1.3 Conclusions	56
4.2 <i>D. DISCOIDEUM</i> KIF5	57
4.2.1 Biochemical properties	57
4.2.2 Cellular localization and function of <i>Kif5</i>	57
4.2.3 Conclusions	58
5 REFERENCES	59
ACKNOWLEDGMENTS	67
CURRICULUM VITAE	68

Summary

The cellular slime mold *Dictyostelium discoideum* contains a total number of 13 kinesins. Two of them, kinesins Kif3 and Kif5, represent the Kinesin-1 family (formerly conventional kinesins) in *D. discoideum* whose members are dimeric molecular motors that move as single molecules micrometer-long distances on microtubules by using the energy from ATP hydrolysis.

In this study constructs of both kinesins were expressed in *E. coli*, purified, and tested in biochemical assays. A GFP-fusion protein of Kif3 revealed an overall cytoplasmic localization with accumulations that could not be assigned to a specific cellular structure or vesicle. Using immunofluorescence staining an association with the endoplasmic reticulum or mitochondria was ruled out. Full-length and truncated Kif3 motors were active in gliding and ATPase assays. They showed a strong dependence on ionic strength. Like the full-length motor, the truncated Kif3-592 motor (amino acids 1-592; comprising motor domain, neck and partial stalk) reached its maximum speed of around $2.0 \mu\text{ms}^{-1}$ at a potassium acetate concentration of 200 mM. The velocity from the microtubule-gliding assay was confirmed using kinesin labeled with Q-Dots. The shortened Kif3-342 motor (amino acids 1-342; comprising motor domain, partial neck) and the Kif3-592 construct showed an ATP turnover comparable to the fungal Nkin motor. Kif3-full-length displayed less activity in ATPase assays, possibly resulting from tail-motor inhibition. Results from the duty ratio calculations and single-molecule gliding assays indicated that Kif3 is a processive enzyme. Overall, *D. discoideum*'s Kif3 revealed a closer similarity to fungal rather than animal kinesins.

The truncated motor Kif5-476 (amino acids 1-476; comprising motor domain, neck and partial stalk) turned out to bind microtubules, but was immotile in gliding assays. Still, this construct, as well as the shorter variant Kif5-353 (amino acids 1-353; comprising motor domain), showed activity in ATPase assays, indicating that a significant portion of the isolated protein was active. Unlike Kif3, the Kif5 motor protein was sensitive to potassium-acetate concentrations exceeding 25 mM and lost its capability to bind microtubules with increasing ionic strength. *D. discoideum* knockout strains showed no apparent phenotype under standard culture conditions or during development. Merely a reduced growth speed was observed in submerged cultures of *kif5*-null cells. A GFP-Kif5 construct showed a strong accumulation in the cell's peripheries, in agreement with previous reports. Microtubule recovery experiments after nocodazole treatment did not reveal any significant differences between wild type and knockout strains, arguing against an influence of Kif5 on microtubule organization.

Abbreviations

ADP	adenosine-5'-diphosphate
AMP-PNP	adenosine-5'-[β , γ -imido]-triphosphate
ATP	adenosine-5'-triphosphat
BCIP	5-bromo-4-chloro-3-indolylphosphat
bp	base pair
BRB80	Brinkmann reconstitution buffer
BSA	bovine serum albumin
C-	carboxy-
cDNA	complementary DNA
DAPI	4',6-Diamidin-2'-phenylindol-dihydrochlorid
DEPC	diethylpyrocarbonate
DNA	deoxyribonucleic acid
dNTP	deoxyribonucleotide triphosphate
DTT	dithiothreitol
EDTA	ethylene diamine tetraacetic acid
EGTA	ethylene glycole tetraacetic acid
FITC	fluorescein isothiocyanat
g	acceleration of free fall
GDP	guanosine-5'-diphosphat
GTP	guanosine-5'-triphosphate
GFP	green fluorescent protein
HEPES	4-(2-hydroxyethyl)-1-piperazine-ethansulfonic acid
ddH ₂ O	double distilled water
IPTG	isopropyl-b-D-1-thiogalactopyranoside
IgG	immunoglobulin G
$K_{bi(ADP)}$	bimolecular binding rate
$K_{bi(ATPase)}$	apparent bimolecular binding rate
K_{bi} ratio	chemical processivity
k_{cat}	catalytic constant
$K_{0.5(MT)}$	half maximal activation constant
NBT	Nitro-blue tetrazolium chloride
Mops	3-(N-morpholino)-propanesulfonic acid
MT	microtubule
MW	molecular weight

N-	amino-
OD	optical density
PAGE	polyacrylamide gel electrophoresis
PBS	phosphate buffered isotonic salt
PCR	„polymerase chain reaction“
PIPES	1,4-piperazindiethan-sulfonic acid
PMSF	phenylmethanesulfonyl fluoride
rpm	revolutions per minute
RT-PCR	reverse transcriptase polymerase chain reaction
SDS	sodium-dodecylsulfate
TBS	N, N, N, N'-tetramethylenediamine
TIRF	total internal reflection fluorescence
Tris	2-amino-2-(hydroxymethyl)propane-1,3-diol
Triton-X-100	t-octylphenoxypolyethoxyethanol
Tween 20	polyoxyethylen-sorbitanmonolaureat
U	international unit for enzyme activity
V_{\max}	maximum rate of extinction decay
V_{gld}	gliding velocity
v/v	volume per volume
w/v	weight (mass) per volume

1 Introduction

1.1 Cytoskeleton and cellular motility

The cell's cytoplasm is filled with protein polymers that prevent deformation and transmit mechanical forces. Three types of proteins build the cytoskeleton: actin, microtubules, and intermediate filaments. While intermediate filaments only prevent excessive stretching of a cell, actin filaments and microtubules do not only resist the mechanical deformation of a cell, but they also serve as “tracks” for most biological movements.

1.1.1 Microtubules

Microtubules are stiff, cylindrical polymers of tubulin. They are 24 nm in diameter and can grow longer than 20 μm in cells and up to millimeters *in vitro*. The subunits of microtubules are heterodimers of α - and β -tubulin. Each subunit binds a guanine nucleotide, either GDP or GTP. The assembly of a microtubule starts at a GTP subunit by a series of biomolecular reactions. The α - and β -tubulin dimers are stacked in linear arrays termed protofilaments, 13 of which form the wall of a microtubule in most cell types.

Due to the uniform orientation of α - and β -tubulin in the polymer, a plus- and a minus-end are distinguishable on the microtubule, calling the exposed β -subunit the plus-end and the α -subunit the minus-end. Association and dissociation of tubulin occurs only at the ends, the plus-end growing faster than the minus-end.

During mitosis microtubules radiate from the cell's two poles towards the sister chromatids and participate in chromosome separation. Although microtubules are in a different organized state during interphase, they also serve as tracks for motor proteins.

1.1.2 Motor proteins

Many organisms depend on motility to stay alive, but it is not only the motility of an entire organism that is of fundamental importance. A variety of essentially important directed movements take place on the intracellular level. One mechanism of this biological movement involves the physical movement of molecular machines on protein polymer tracks. The needed energy is released directly by the hydrolysis of adenosine triphosphate (ATP) in a specialized domain of the cytoskeletal motor protein named the head, which also contains the binding region for the track. After ATP hydrolysis the motor protein will take several nanometer wide steps on its track.

Three different classes of cytoskeletal motors have evolved: the myosins, which use actin filaments as tracks, and two classes of microtubule dependent motors, kinesins and

dyneins. The actin-myosin system is responsible for muscle contraction, cytokinesis, and organelle movements in plants. Microtubule motors on the other hand power the beating of cilia and flagella, chromosome separation during mitosis, and the transport of many different cellular components to specific destinations within the cytoplasm and between membrane bound compartments. The majority of kinesins moves towards the plus-end of microtubules, but known exceptions are the members of the Kinesin-14 family, who move towards the minus end.

1.1.2.1 The kinesin superfamily

Since the long range transport of organelles and vesicles in neuronal or epithelial cells is of fundamental importance, it is not surprising that the first kinesin motor protein was identified in the giant squid axon as a motile force that underlies the movement of particles along microtubules (Brady, 1985; Vale et al., 1985b). Since then a systematic search has identified 17 subfamilies (Dagenbach and Endow, 2004; Hirokawa et al., 1998; Schliwa, 2003; Wickstead and Gull, 2006) belonging to the superfamily of kinesins.

Reported members of the animal and fungal kinesin families have a motor domain attached through a neck and a stalk region to a variety of tails that interact with cargoes. With only some variation in the amino acid sequence, the motor unit is highly conserved throughout the kinesin family and shows an evolutionary relationship to the catalytic domains of myosin and G proteins (Vale, 1996). The classification of kinesin proteins is mainly based on these sequence similarities in the ATP-binding, -hydrolyzing, and microtubule-binding sites. Another feature to distinguish kinesins is the position of the motor domain which can be either located at the amino-terminus, the carboxy-terminus, or internal within the polypeptide chain. Regions outside the motor domain where protein-protein interactions occur with accessory light chains or other interacting proteins lead to further diversity (Goldstein, 2001).

Functions described for members of the kinesin superfamily include transport of vesicles, organelles, chromosomes, protein complexes, and RNPs, as well as regulatory functions in microtubule dynamics (Hirokawa, 1998; Soldati and Schliwa, 2006). The Kinesin-14 family member Kar3 for example is one of the regulators that promote transport of captured kinetochores along microtubules by not only translocating along the microtubules, but also by catalyzing microtubule depolymerization (Sproul et al., 2005). Kar3 thereby uses its motor domain for both modes of force production, translocation and depolymerization.

The kinesin superfamily has become so large that several different naming schemes have emerged over time. In order to avoid further confusion, a standardized kinesin nomenclature was introduced in 2004 (Lawrence et al., 2004). Each family bears the name “kinesin” which arises from the Greek word “kinein”, meaning “to move” (Brady et al., 1985; Vale et al., 1985a), followed by an Arabic number to designate each family.

1.1.2.1.1 The Kinesin-1 family or formerly conventional kinesins

The first kinesin to be identified was also called conventional kinesin, a homodimer of two heavy chains, each of which possesses an amino-terminal motor domain, a long stalk with alternating flexible and coiled-coil structures, and a small globular tail domain (Figure 1). The two motor domains or heads bind mostly to the β -subunit of tubulin and move processively along microtubules, meaning that at each time point the dimeric molecule is tethered to the microtubule by at least one of its two heads (Ray et al., 1993; Woehlke et al., 1997).

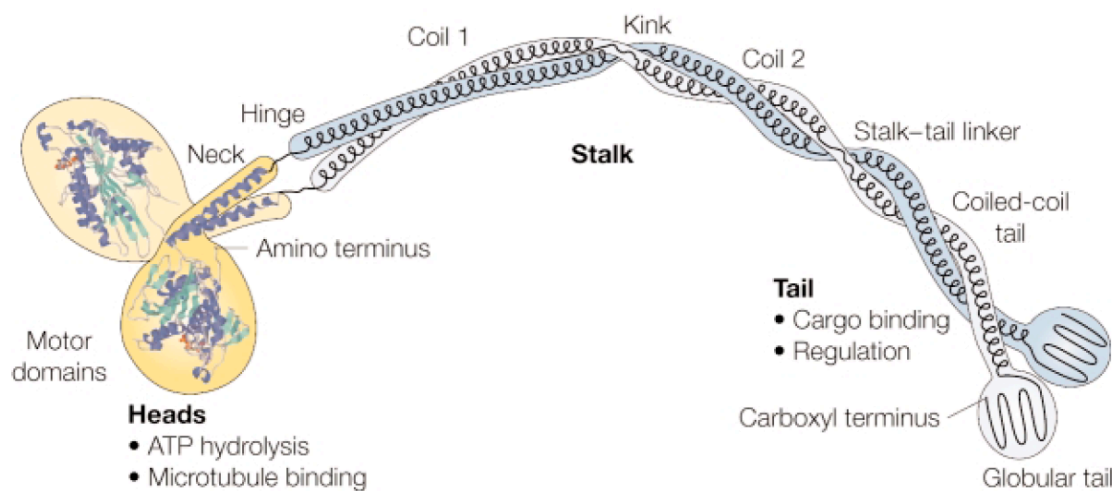


Figure 1: Domain organization of the conventional kinesin heavy-chain dimer (Woehlke and Schliwa, 2000). The catalytic head, the neck-linker, and the coiled-coil neck domain show the crystal structure of the rat kinesin dimer (Kozielski et al., 1997). The other domains are based on electron microscopic images (Hirokawa et al., 1989; Schliwa, 1989).

1.1.2.1.2 The hand-over-hand model of kinesin motility

The most intriguing property of conventional kinesins is their impressive processivity, which allows them to take several hundred steps along the microtubule track before falling off, and by this facilitating the transport of cargo over long distances.

Throughout the catalytic cycle one head is kept in a tight microtubule-bound form, containing either ATP or no nucleotide, while the other head is in transit in an ADP-bound form. Both heads are bound to the microtubule only during a brief phase of the cycle. In the asymmetric hand-over-hand model the heads exchange leading and trailing roles with each step. The rear head detaches from the microtubule, moves to the front and attaches again. A strict catalytic and mechanical alternation during this processive movement is needed in order to keep the heads working in concert (Figure 2) (Asbury, 2005; Valentine and Gilbert, 2007; Yildiz and Selvin, 2005).

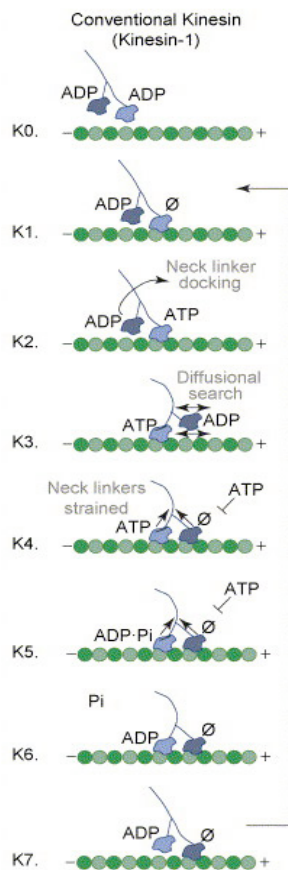


Figure 2: Hand-over-hand model of conventional kinesin. In solution both motor heads tightly bind ADP (K0). Upon filament binding of the first head (head one), ADP is released (K1) and the motor enters a strongly microtubule-bound and nucleotide free state. Subsequently, ATP binds to the active site of head one, which leads to docking of the neck-linker (K2) and movement of head two towards the plus end of the microtubule (K3). After diffusional search head two binds to the microtubule and releases its ADP, leading to an intermediate state with both heads tightly bound and the neck linker strained (K4). Exiting this intermediate state must be strongly regulated since premature binding of ATP to the empty binding site of head two would desynchronize the catalytic cycle of the motor protein and eventually lead to microtubule dissociation. After ATP hydrolysis (K5) and release of P_i , head one enters a weak binding state (K6) and detaches from the microtubule, restating the catalytic cycle with alternated positions (K7) (Valentine and Gilbert, 2007).

The heads are functionally equivalent, but out of phase from the biochemical point of view. In addition the head's steps differ: the moving head always passes on alternate sides of the attached head. A flexible structure, possibly the hinge that connects the head to the stalk, suppresses strong pivoting that would occur when the heads swap places (Asbury et al., 2003; Kaseda et al., 2003; Yildiz et al., 2004).

Although the model shown in Figure 2 is representative of published results, points of disagreement remain. For example kinesin motors pause in a so-called “waiting” state between the conformational changes that drive processive stepping. During this state the rear ADP-containing head (steps K1 and K6-K7) can infrequently synthesize ATP, suggesting that, in contrast to the model, tight microtubule binding occurs (Hackney, 2005). On the other hand, force measurements (Uemura et al., 2002), mechanical (Carter and Cross, 2005), and kinetic data (Auerbach and Johnson, 2005) suggest that during the “waiting” state, one head binds to the microtubule while the other diffuses. Another controversy surrounds kinesin's ability to step backwards along a microtubule towards the minus-end (Svoboda et al., 1994). Recent results showed that at high superstall forces, kinesin would step processively backwards in an ATP-dependent manner (Carter and Cross, 2005). A model was proposed in which the heads being forced to step backwards in order to promote the dissociation of incorrect nucleotides or to reorient an incorrectly positioned neck linker to reset the coordination between both motor heads (Valentine and Gilbert, 2007).

1.2 *Dictyostelium discoideum*

Dictyostelium discoideum is a powerful system for basic research in cell and developmental biology. The natural habitat of *D. discoideum* is the deciduous forest soil, where it feeds on bacteria and multiplies by equal mitotic division. The single independent cells can interact to form a multicellular structure when challenged by adverse conditions such as starvation. More than 100,000 cells aggregate by chemotaxis towards a cAMP gradient to form a mound that is surrounded by an extracellular matrix. About one third of the cells sacrifice themselves as stalk cells for the survival of the rest of the population explaining why *D. discoideum* is also called the social amoeba (Fortunato et al., 2003; Schaap et al., 2006). Figure 3 shows its life cycle.

A good resource for genetic information and molecular methods in the world-wide-web is the webpage www.dictybase.org, supported by a growing community of researchers. The publication of the entire *D. discoideum* genome in 2005 significantly facilitated the performance of proteomic studies. Despite their apparent simplicity many genes of *D. discoideum*'s 34 Mb genome show a high degree of sequence similarity to related species such as *Neurospora crassa* (Eichinger and Noegel, 2005). The gene-dense chromosomes encode approximately 12,500 predicted proteins.

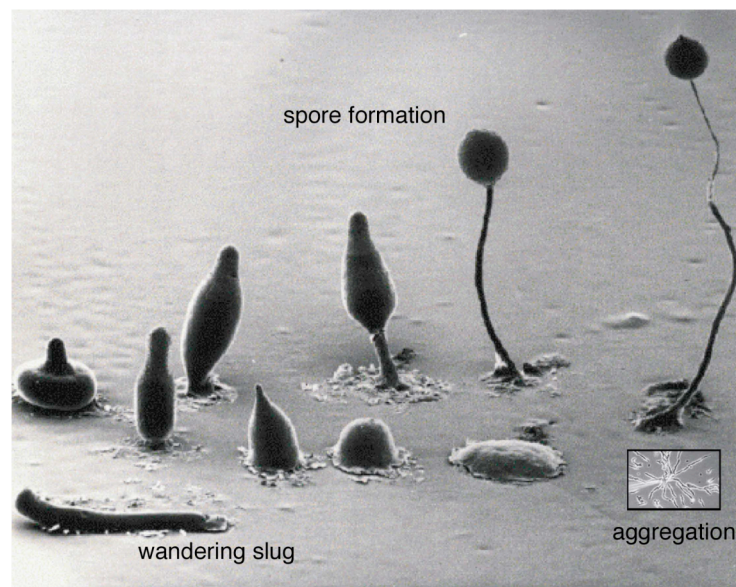


Figure 3: Life cycle of *D. discoideum* (REM-photographs from M. J. Grimson und R. L. Blanton, Biological Sciences Electron Microscopy Laboratory, Texas Tech University). During growth phase *D. discoideum* exists as single cell amoeba. Upon starvation cells undergo chemotaxis and form the mound. A finger like structure emerges and forms either immediately a fruiting body or a motile slug.

A genome-based phylogeny showed that the amoebozoa diverged from the animal-fungal lineage after the plant-animal split, but *D. discoideum* seems to have retained more of the diversity of the ancestral genome than have plants, animals or fungi (Eichinger et al., 2005).

D. discoideum cells are easy to grow, lyse, and process for a multitude of biochemical, molecular genetic, and cell biological assays. The organism is uniquely suited for studies of cytokinesis, motility, phagocytosis, chemotaxis, signal transduction, and aspects of development. Many of these processes, which play important roles in health and disease are either absent or are less accessible in other model organisms. Molecular genetic techniques in this work include gene inactivation by homologous recombination, and the expression of fluorescent fusion proteins.

In *D. discoideum* microtubules are organized as radial arrays emanating from a single microtubule-organizing center (Roos et al., 1984). The arrays are not as robust in numbers (30 – 70 microtubules per centrosome (Kimble et al., 2000)) or as dynamic as in other systems, but they do support a large volume of intracellular traffic (Ma et al., 2001; Roos, 1987).

Once nucleated, interphase microtubules in *D. discoideum* appear to remain firmly anchored by their presumed minus-ends to the centrosome. Contrary to mammalian cells, the microtubule arrays share a common cytoplasm but maintain a roughly uniform distance from another with minimal overlaps between their distal ends (Koonce and Khodjakov, 2002). Upon entrance of the cell into mitosis, the radially arranged microtubules immediately break down and the mitotic spindle is formed as a compact bar-shaped structure between the two separating centrosomes. Spindle microtubules are nucleated from surfaces that were previously buried inside the interphase centrosome (Ueda et al., 1999). The spindle microtubules then attach to the six *D. discoideum* chromosomes via distinct kinetochores that show architectural characteristics comparable to those of higher eukaryotes (McIntosh et al., 1985), and subsequently separate the chromosomes.

Interestingly, a disruption of the microtubule cytoskeleton prevents mitosis as expected, but shows no major defects during interphase. A *D. discoideum* DdLIS1 point mutant lacks an ordinary distribution of microtubules, but grows normally on bacterial lawn and in culture medium, indicating normal phago- and pinocytosis. Even an inhibition in cellular movement could not be detected (Rehberg et al., 2005). On the other hand live *D. discoideum* cells show a large amount of rapid linear organelle motion on microtubule tracks and this movement halts after addition of the microtubule depolymerization reagent nocodazole (Roos, 1987). Taken together, these contrary observations make it even harder to determine the significance of *D. discoideum*'s interphase microtubule network for the survival of the organism.

1.3 Kinesins in *Dictyostelium*

Homology searches for the kinesin motor domain in the *D. discoideum* genome (Eichinger, 2003) led to the identification of thirteen *Dictyostelium* kinesins (Kollmar and Glockner, 2003). The acronym “Kif” followed by a number was given to all kinesins, in compliance with the nomenclature of human and mouse kinesins.

According to the authors and based on phylogenetic analysis, three *D. discoideum* kinesins (Kif3, Kif5, Kif7) group to the Kinesin-1 (conventional kinesin) subfamily that is implicated in organelle transport. Kif7 shows a close homology to conventional kinesins but it remains to be elucidated if it really reveals conventional kinesin properties. The kinesin Unc104 was recently grouped to the Kinesin-3 superfamily (Wickstead and Gull, 2006), in which the Unc104 homologs of *Caenorhabditis elegans* and *Drosophila melanogaster* can also be found.

Six kinesin motor proteins belong to subgroups predicted to function exclusively during mitosis (Kif2, Kif4, Kif6, Kif11, Kif12, Kif13), and two have multiple functions, that is mitosis and organelle transport, depending on the stages of the cell cycle (Kif8, Kif10). One kinesin could not be grouped with any of the other known kinesins (Kif9) (Figure 4).

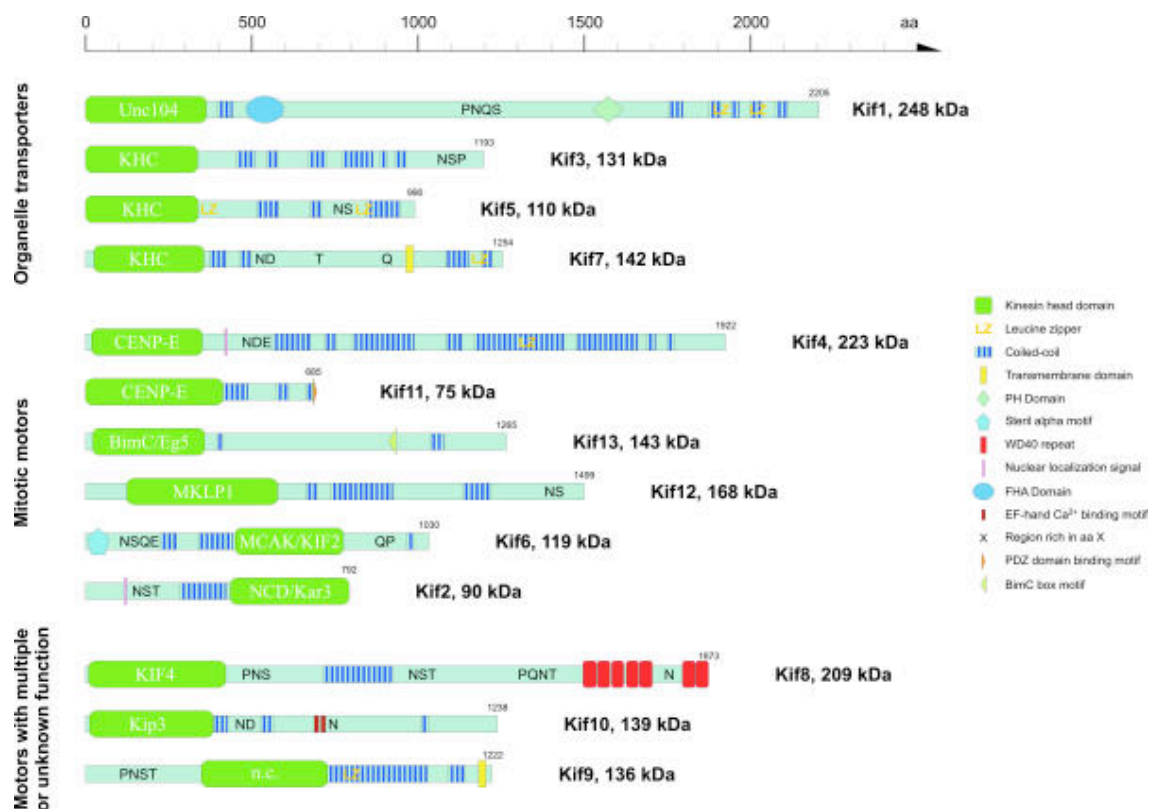


Figure 4: Schematic diagram of the domain structures of *Dictyostelium* kinesins (Kollmar and Glockner, 2003). Conventional kinesins Kif3 and Kif5 are grouped to the organelle transporters.

Little is known about *D. discoideum*'s conventional kinesins. Like fungal but unlike metazoan kinesins they lack accessory light chains (Grummt et al., 1998; Jeong et al., 2002; Steinberg and Schliwa, 1995) and their ability to induce organelle transport *in vitro* suggests that they are involved in membrane transport, like their fungal and metazoan orthologous (Klopfenstein et al., 2002).

1.3.1 Kif3 (Kinesin-1 subfamily)

This 131 kDa kinesin was first described in 1998 (de Hostos et al., 1998) and contains an N-terminal motor domain followed by a 30 aa linker consisting of only glycine and serine residues. The neck is connected to a long α -helical domain composed of coiled-coil regions, the stalk. The C-terminal tail is thought to be free from secondary structural elements. Kif3 has been found to co-fractionate occasionally with vesicle preparations but the nature of the isolated vesicles is unknown (Pollock et al., 1999).

1.3.2 Kif5 (Kinesin-1 subfamily)

Kif5 has a molecular mass of 110 kDa and is the *D. discoideum* kinesin most similar to human conventional kinesin, sharing 52 % identity in the motor domain (Navone et al., 1992). It was first described in 2004 (Iwai et al., 2004) and consists of an N-terminal motor domain, a central stalk region, and a C-terminal tail domain. Its ability to form dimers is enhanced by two leucine zippers.

The C-terminal tail domain directly interacts with actin filaments and bundles them *in vitro*. As expected, the motor domain showed binding to microtubules in an ATP-dependent manner, suggesting that Kif5 may connect microtubules to actin filaments (Iwai et al., 2004).

Immunofluorescence microscopy showed an enrichment of Kif5 at actin-rich cell surface protrusions such as pseudopodia and also a weak distribution throughout the cytoplasm. A Kif5-null cell line exhibited no obvious phenotype, suggesting that the *kif5* gene is not essential for the growth and development of *D. discoideum* cells under laboratory conditions (Iwai et al., 2004).

1.4 Aims of the work

The genome of *D. discoideum* contains 13 genes for kinesin-related proteins (Kollmar and Glockner, 2003), among them two that encode Kinesin-1 family members. One, Kif5, is a kinesin that seems to link microtubules and actin (Iwai et al., 2004), the other one, Kif3, is largely uncharacterized.

A phylogenetic classification based on structural data and the specific biochemical behavior should shed light on aspects of kinesin evolution.

The determination of the biochemical properties, as well as the cellular localization and the identification of the potential cargo from both kinesins was the primary goal. In this study both kinesins were recombinantly expressed and characterized using biochemical, molecular biology, and cell-biology methods.

2 Materials & Methods

2.1 Materials

2.1.1 Reagents and other materials

Unless stated otherwise chemicals were obtained from BioRad (München), Fluka (Buchs, Schweiz), Merck (Braunschweig), Roche Diagnostics (Penzberg), Carl Roth (Karlsruhe), Serva (Heidelberg); Sigma-Aldrich (Deisenhofen) and were of p.a. quality.

2.1.2 Vectors

pA6PGFP-L-SSEB *D. discoideum* expression, actin6 promoter (Graf et al., 2003)

pDiscGFPSSEB2 *D. discoideum* expression, discoidin promoter (Daunderer and Graf, 2002)

339-3 Sal mRFPmars *D. discoideum* expression, actin15 promoter, based on mRFPmars in pBsrH (Fischer et al., 2004), *EcoRI* site exchanged versus *SalI* site

pDiscCitrineSSEB2 *D. discoideum* expression, discoidin promoter, based on pDiscGFPSSEB2 (Daunderer and Graf, 2002), sgGFP-cassette exchanged versus Citrine cassette derived from mCit-N1 (CLONTECH Laboratories Inc., Mountain View, CA, USA)

pLPBLP [floxed Bsr] *D. discoideum* expression, actin6 promoter (Faix et al., 2004)

pBluescript II KS *E. coli* expression, T3/T7 promoter Stratagene (Heidelberg)

pET-24b *E. coli* expression, T7 promoter Novagen (Merck, Darmstadt)

2.1.3 Antibodies

Pineda Antikörper-Service (Berlin) generated the Kif3-342 polyclonal antibody in rabbits.

Calnexin 270-390-2 monoclonal antibody (Muller-Taubenberger et al., 2001)

anti-tubulin, mAb YL1/2 Chemicon (Millipore, Schwalbach)

anti-GFP, rabbit antiserum (Faix et al., 2001)

anti-porin 70-100-1	(Troll et al., 1992)
goat-anti-rat Alexa 488 or 568	Molecular Probes (Invitrogen, Karlsruhe)
goat-anti-rabbit IgG antibody Cy3	Dianova (Hamburg)

2.1.4 Other markers

phalloidin Alexa 635	Invitrogen (Karlsruhe)
----------------------	------------------------

2.2 Organisms

2.2.1 *D. discoideum* strains

D. discoideum strain AX2-214, axenic growing derivate of isolate NC-1 (Raper, 1935), was used in this study.

An AX2 cell line with GFP-tagged mitochondria was kindly provided. DMIF1, an inhibitor protein of the mitochondrial F_1F_0 -ATPase was ligated into the expression vector pDEXRH-N-GFP (Westphal et al., 1997) to obtain a C-terminal GFP-construct, which localizes to mitochondria only (unpublished Ph.D. thesis of A. Huettig, Technical University Munich, 2004).

2.2.2 Media and cultivation of *D. discoideum*

D. discoideum cells were cultured axenically in AX-medium on a rotary shaker at 150 rpm and 21°C. The medium contained blasticidin S or G418 respectively in a concentration of 10 µg/ml. Backup cultures of adherent cells were kept in HL5c medium in small tissue culture flasks and medium was changed twice a week.

For long term storage cells were subjected to starving conditions, inducing the formation of spores, which can easily be frozen and stored. For this, axenically growing cells were washed twice with Soerensen buffer, suspended at a density of $2-3 \times 10^8$ cells/ml and 500 µl of the suspension were plated on freshly prepared phosphate agar plates. Cells formed spores containing fruiting bodies within 2-3 days, which were washed off with sterile Soerensen buffer (about 4 ml per plate), and stored at -70°C. For inoculation of a shaking culture, spores were thawed at room temperature and resuspended in 30 ml HL5c medium. Within 3 days the cultures usually reached a density of about 5×10^6 cells/ml.

AX medium

14.3 g/l Peptone, 7.15 g/l yeast extract, 18 g/l glucose, 3.5 mM Na₂HPO₄, 3.5 mM KH₂PO₄; pH 6.7

HL5c medium (Claviez et al., 1982)

5 g/l yeast extract (BD Biosciences, New Jersey, USA), 2.5 g/l bacto tryptone (BD Biosciences), 2.5 g/l caseine peptone, 5 g/l proteose peptone (BD Biosciences), 10 g/l glucose, 1.2 g/l KH₂PO₄, 0.35 g/l Na₂HPO₄; pH 6.5

Phosphate buffer (Soerensen) (Malchow et al., 1972)

14.6 mM KH₂PO₄, 2 mM Na₂HPO₄; pH 6.0

Phosphate-agar plates

15 g/l bacto agar in phosphate buffer.

SM agar plates

10 g/l peptone, 1 g/l yeast extract, 10 g/l glucose, 9 g/l bacto Agar, 16 mM K₂HPO₄, 5.7 mM KH₂PO₄, 4 mM MgSO₄; pH 6.5

Electroporation buffer

50 mM sucrose, 10 mM KH₂PO₄; pH 6.1

2.2.3 Bacterial strains

Escherichia coli strains DH5 α (Sambrook, 1989) and XL1-Blue (Stratagene, Heidelberg) were used for cloning. *E. coli* strain BL21CodonPlus (DE)-RIL (Studier et al., 1990) (Stratagene) was used for protein expressions.

2.2.4 Media and cultivation of *E. coli*

E. coli cells were grown according to standard methods (Sambrook, 1989) on agar plates or shaking cultures (220 rpm, 37°C). For protein expression the temperature was reduced to 16°C.

For long-term storage at -70°C, 50 % glycerol was added to the liquid cultures.

LB medium

10 g/l tryptone, 5 g/l yeast extract, 10 g/l NaCl; pH 7.0

For solid medium 1.5 % agar was added. If necessary, ampicillin or kanamycin was added from stock solutions to a final concentration of 100 μ g/ml.

SOC

20 g/l tryptone, 5 g/l yeast extract, 10 mM NaCl, 2.5 mM KCl, 10 mM MgCl₂, 10 mM MgSO₄, 20 mM glucose

TPM

20 g/l tryptone, 15 g/l yeast extract, 8 g/l NaCl, 2.5 g/l Na₂HPO₄, 1 g/l KH₂PO₄, add 0.2 % glucose after autoclaving

2.3 Molecular biology methods

2.3.1 Agarose gel electrophoresis

DNA fragments were separated on agarose gels containing 0.8 % to 1.2 % agarose (Invitrogen) in TAE buffer. To visualize the DNA fragments 0.05 µg/ml ethidium bromide was added to the liquid agarose. The DNA samples were mixed with Laemmli buffer before loading on the gel. For size separation of the DNA fragments a voltage of 75 V was applied to the agarose gels. Bands were detected by UV illumination and documented using the Eagle Eye II CCD camera system (Stratagene).

50 x TAE

2 M Tris-HCl, 0.57 % acetic acid, 50 mM EDTA; pH 7.5

6 x Laemmli buffer

30 % glycerol, 0.25 % bromphenol blue, 0.25 % xylene cyanol

2.3.2 DNA extraction from agarose gels

DNA bands were excised from agarose gels with a scalpel, transferred into a sterile Eppendorf vial and purified using the “Qiaquick gel extraction kit” (Qiagen, Hilden), following the instructions of the manufacturer. The DNA was resolved in 30 µl Qiagen’s elution buffer.

2.3.3 Determination of DNA concentrations

The concentration of DNA solutions was determined in the photometer via the extinction at 260 nm (E_{260}), with $E_{260} = 1.0$ corresponding to 50 µg/ml double-stranded DNA.

2.3.4 Preparation of plasmid DNA

Plasmid DNA was prepared from overnight shaking cultures using the Qiagen-Plasmid-Kit (Qiagen). The manufacturer’s manuals for mini- (3 ml), midi- (50 ml) or maxi-preparations (200 ml) were followed. The DNA was dissolved in ddH₂O.

2.3.5 Preparation of chromosomal DNA

1-2 x 10⁸ axenically growing *D. discoideum* cells were washed twice with cold H₂O, then centrifuged and resuspended in 50 ml lysis buffer. The nuclei were sedimented at 6,000 g (JA20, 7,500 rpm, 10 min, 4°C) and resuspended in SDS lysis buffer (TE buffer

with 0.7 % SDS). After addition of 100 µl proteinase K solution (14,7 mg/ml) the lysate was incubated for 2-3 h at 60°C and subsequently extracted with phenol and chloroform until the upper phase appeared to be clear (2-4 repeats). The DNA was precipitated by the addition of 1/10 volume of 2 M Na-acetate (pH 5.2) and 2 volumes of ethanol. DNA fibers were wound up with a pipette tip and washed in 70 % ethanol, and then air dried, and dissolved in 200-500 µl TE buffer.

Small amounts of genomic DNA for PCR analysis of clones were isolated using the “high pure PCR template preparation” kit (Roche Diagnostics, Basel).

Lysis buffer

10 mM Mg-acetate, 10 mM NaCl, 30 mM HEPES·NaOH pH 7.5, 10 % sucrose,
2 % Nonidet P40

TE buffer

10 mM Tris, 1 mM EDTA; pH 8.0

2.3.6 Isolation of polyadenylated RNA

Polyadenylated RNA (mRNA) was isolated from *D. discoideum* cells using the “QuickPrep *micro* mRNA Purification Kit” from Amersham Biosciences (Buckinghamshire, UK). The mRNA was precipitated in 2 to 4 aliquots with 1/10 volume 2 M K-Acetate, 2 volumes of ethanol, and glycogen. Precipitated mRNA was eventually stored at -70°C. Further usage as template for RT-PCR required the recovery of the mRNA by centrifugation (14,000 rpm; 15 min; 4°C; Beckman CS-15R centrifuge, F2402 Rotor), washing in 70 % ethanol (in DEPC treated water), and air drying before dissolving in DEPC treated water.

The yield was usually between 5 and 6 µg per 1×10^7 cells and was determined at 260 nm in the photometer.

2.3.7 Polymerase chain reaction (PCR)

For standard PCR reactions the “Expand High Fidelity Polymerase Mix” (Roche Diagnostics) was used. The reaction mixture contained the standard reaction buffer with 2 mM MgCl₂, approximately 10 ng template DNA, 200 mM of each dNTP, 0.5 µM 5'- and 3'-primer and 1 unit Expand-Polymerase (Roche Diagnostics) in a volume of 50 µl. The number of reaction cycles and the temperature of denaturation, annealing, and elongation phases were chosen according to the supplier's instruction.

2.3.8 Reverse transcription PCR (RT-PCR)

500 ng of polyadenylated RNA were mixed with 2 pmol of a gene specific primer in a total volume of 14 µl, denatured for 5 min at 70°C and immediately chilled on ice for 5 min. Reverse transcription was initiated by the addition of 5 µl 5 x RT-buffer, 10 mM of each dNTP, and 50 units of M-MLV Reverse Transcriptase (Promega, Madison, WI,

USA). The reaction was carried out in a thermal cycler at 42°C for 60 min, and subsequently terminated by heating to 70°C for 15 min.

2 µl of the reverse transcription reaction were used as template in subsequent PCR amplifications.

2.3.9 DNA cleavage with restriction enzymes

Restriction endonucleases were obtained from New England Biolabs (NEB, Ipswich, MA, USA). Restriction digests were performed using the buffer and temperature recommended by the manufacturer. At least 4 units of enzyme were used per µg DNA. The reaction volume was at least 25 µl. Samples were incubated at least 1 h and analyzed on agarose gels.

2.3.10 Site directed mutagenesis

In order to mutate specific sites on the genome PCR with *PfuTurbo* DNA polymerase (Stratagene) was performed on the plasmid of choice, using a modifying oligonucleotide containing the mutated bases and approximately 20 bp in each direction. In order to remove the bacterial template DNA that did not contain the intended mutation, the product was cleaved with *DpnI*, which specifically cleaves methylated DNA. The cleaved PCR product was directly transformed into *E. coli* cells. Clones containing introduced mutations were verified by sequencing.

2.3.11 Ligation

Vector and DNA were cleaved by the appropriate endonucleases, separated on agarose gels, and extracted from them. The vector was dephosphorylated by Antarctic phosphatase (NEB) to prevent re-ligation. Double amount and the fourfold molar excess of insert were incubated with 50 ng of vector DNA and ddH₂O in a volume of 10 µl at 56°C for 2 min and subsequently chilled on ice for 5 min.

The ligation was started by adding T4 DNA ligase (NEB) and its supplied buffer in a volume of 5 µl to the vector-DNA mix at 16°C for at least 2 h or over night. 50 ng of vector DNA were incubated without insert as re-ligation control.

2.3.12 Preparation and transformation of competent cells

2.3.12.1 Preparation of electrocompetent cells

1 l LB medium was inoculated with 10 ml of an electro competent XL1blue *E. coli* overnight culture and grown at 37°C, shaking at 220 rpm to an OD₆₀₀ of 0.6. Subsequently, the culture was cooled to 4°C. The bacteria were harvested by centrifugation (GSA rotor: 4,000 rpm, 15 min, 4°C) and resuspended in 1 l H₂O. After a further centrifugation step the cells were resuspended in 500 ml H₂O, centrifuged again, washed with 10 % glycerol and finally resuspended in 3 ml of 10 % glycerol. After

aliquotation the bacteria suspension was shock frozen in liquid nitrogen and stored at -70°C.

2.3.12.2 Electroporation

For transformation 50 µl of electro competent cells were thawed on ice and mixed with 50 ng of vector DNA or 2.0 µl of ligation reaction and placed in a pre-cooled, sterile 2 mm electroporation cuvette (Eurogentec, Serain, Belgium). After a pulse (2.5 kV, 25 mF) the whole cell suspension was mixed with 300 µl pre-cooled SOC medium. The cells were then placed for one hour under shaking into an Eppendorf incubator at 37°C. After the incubation the cells were plated on LB agar plates supplied with the appropriate antibiotics.

2.3.12.3 Preparation of competent cells

Competent cells were prepared following the instructions of Inoue (Inoue et al., 1990). 250 ml SOB medium was inoculated with 3 ml of a BL21 CodonPlus (DE)-RIL *E. coli* overnight culture and grown to an OD₆₀₀ of 0.6 at 37°C under vigorous shaking. This culture was cooled on ice for 10 min and the cells were harvested by centrifugation (GSA rotor: 2,500 rpm, 10 min, 4°C) and resuspended in cold PIPES buffer. After another centrifugation step the cells were resuspended in 20 ml PIPES buffer and 7 % DMSO (v/v). The cell suspension was fractionated into 50 µl aliquots, shock frozen in liquid nitrogen, and stored at -70°C.

Resuspension buffer

10 mM PIPES·KOH, 55 mM MnCl₂, 15 mM CaCl₂, 250 mM KCl; pH 6.7

2.3.12.4 Heat shock transformation

SEM competent cells were thawed on ice. 50 µl of cells were mixed with 5.0 µl ligation reaction and incubated on ice for 30 min. Subsequently, the mixture was placed in a 42°C water bath for 45 sec, cooled on ice for 5 min, and mixed with 300 µl pre-cooled SOC medium. The cells were then placed for one hour under shaking into an Eppendorf incubator at 37°C. The cells were plated on LB agar plates supplied with the appropriate antibiotics.

2.3.13 Colony check PCR

Colony check PCR was performed by preparing 10 µl PCR master mixes containing 6.1 µl of ddH₂O, 1.0 µl of 10 x PCR buffer, 0.8 µl nucleotide mix, and 1.0 µl of each Primer (usually T7 and T7terminator). A single colony was collected with a toothpick, dipped into the PCR-mix and put into 3 ml LB medium with the appropriate antibiotic. The PCR was analyzed on an agarose gel and positive clones transferred from the 3 ml pre-culture to 50 or 200 ml cultures for midi or maxi preps, respectively. Plasmids were then sequenced by AGOWA, Berlin. Sequences were analyzed using DNA Strider 1.4f6, CEA France.

Alternatively DNA of transformed bacteria was isolated, cleaved with appropriate restriction endonucleases and analyzed on agarose gels. Plasmids with restriction fragments of the expected size were also sequenced by AGOWA, Berlin.

2.3.14 Construction of null-mutants

All constructs were generated by PCR on gDNA. PCR products were purified from 1.0 % agarose gels and cloned into the knockout vector pLPBLP [floxed Bsr].

Table 1: Primers used for constructing null-mutants.

Construct name	Primer forward	Primer revers
KOKif3 Construct1_5'	CGGGATCCAATAAATAATACCTTCGCTCC	AACTGCAGATCTACAACTACTCTAATCGA TGAC
KOKif3 Construct1_3'	GCGCGTCGACAAGCTTGACAGGTATTAA TGATCCAAATGG	GGGGTACCCAGTTACACCTGAAACAGTCT C
KOKif3 Construct2_5'	CGGGATCCCGATGTCATCGATTAGAGTA GTTTGTAG	AACTGCAGGGTACTATACCTCTTAACTCTT G
KOKif3 Construct2_3'	CCCAAGCTTGGGTGTTTCAGCACCAACA TCACC	CATCTGCATGTTTGAAGCGG
KOKif5 Construct1_5'	CGGGATCCCGAAACCCTATGATACTATTA TCGGCATATTTTTTAAATG	AACTGCAGGTTATTATTATAATATTATTTCA TCTAAGAGGAAATTTTC
KOKif5 Construct1_3'	CCCAAGCTTGAGGAGTATGTAGCAAGTG AAGAGG	GGGTACCCCAATTCTTTTGGTATTGGATTA CCAGG

KOKif3 construct 1:

First the 5' construct was cloned into the pLPBLP-vector using *Bam*HI and *Pst*I restriction sites. The 3' construct was added using *Kpn*I and *Hind*III restriction sites after proving the correct orientation of the first insert by PCR.

KOKif3 construct 2:

The same restriction sites and the same order of cloning as for construct 1 apply for construct 2.

KOKif5 construct 1:

The same restriction sites and the same order of cloning as for the Kif3 constructs apply for the Kif5 construct 1.

2.3.15 Generation of expression constructs

All constructs were generated by PCR on either cDNA or gDNA, respectively. PCR products were purified from 1.0 % agarose gels and cloned either directly into the expression vector system or with blunted ends via the pBluescriptII KS vector (Stratagene).

Table 2: Primers used for constructing expression constructs.

Construct name	Primer forward	Primer revers	Vector
Kif3-342	GGAATTCCATATGTCATCGATTA GAGTAGTTTGTAG	CGGGATCCCAGCAGCACTTCTTTC TTG	pET24b
Kif3-592	GGAATTCCATATGTCATCGATTA GAGTAGTTTGTAG	CATCTGCATGTTTTGAAGCGG	pET24b
Kif3-full length 5'	GGAATTCCATATGTCATCGATTA GAGTAGTTTGTAG	CATCTGCATGTTTTGAAGCGG	pET24b
Kif3-full length 3'	CAAAGTGGTGATTCTCAATCGC	GCGAGCTCCTAGTTACAACGTCAG GAGTATATGAGAAATTGACAGG	pET24b
Kif5-head	CTTGTTTATAATGGTACACTTTTA GCGTATGGTCAAACAGG	CGGGATCCCGGCAGCACTTTTCTC TTG	pET24b
Kif5-truncated	GGAATTCCATATGGCAACAAGTT GTAATATTAGAGTAATGTGTAGG	GCCCAAGCTTCTAATGTGTTGATG CTGATGAATGTGG	pET24b
GFP Kif3-full 5'	GACGCGTCGACGCTCATCGATT AGAGTAGTTTGTAG	CATCTGCATGTTTTGAAGCGG	pA6PGFP- SSEB
GFP Kif3-full 3'	CAAAGTGGTGATTCTCAATCGC	CGGGATCCCTAATCTTTTTGTTGAT CTTTGTTAATTGTTG	pA6PGFP- SSEB
GFP Kif5-full	GACGCGTCGACTCGCAACAAGT TGTAATATTAGAGTAATGTGTAG G	CGGGATCCTTTAATTATTGAAAAAG TGTTTACTATTTTCAG	pA6PGFP- SSEB
RFP Kif3-tail	CAAAGTGGTTCCTCAATCGC	GGATATCCTAATCTTTTTGTTGATC TTTGTTAATTG	339-3 Sal mRFPmars
Citrine Kif3-342	GAGATCTAAAATGGTGAGCAAG GGCGAGGAGCTGTTC	CGGTCGACACATATGTCCTCCGGA CTTGACAGCTCGTCCATGCC	pDiscCitrineSS EB2

Kif3-342:

The purified PCR product was cloned directly into the pET24b expression system using *NdeI* and *BamHI* as restriction sites.

Kif3-592:

The purified PCR product was cloned with blunt ends into the pBluescript II KS vector (cut with *EcoRV*, purified from 1.0 % agarose gel and dephosphorylated with Antarctic phosphatase). After the insert was proven by colony-check PCR, plasmid midi preps were prepared of the positive clones and a sample was sequenced (AGOWA, Berlin). Plasmids with correct sequence were digested with *NdeI* and *BamHI*, separated on a 1.0 % agarose gel, purified with the QIAquick Spin kit (Qiagen) and ligated into the pET24b expression system (cut with *NdeI* and *BamHI*, purified from 1.0 % agarose gel and dephosphorylated with Antarctic phosphatase). Positive clones were identified by PCR and plasmids were sequenced.

Kif3-full-length 5' and 3':

The purified PCR products were cloned with blunt ends into the pBluescript II KS vector (see above). The 5' construct was cloned first into the pET24b expression system using *NdeI* and *BamHI*. After colony check PCR and sequencing the pET24b vector with the 5' construct was digested with *BamHI*, purified with QIAquick Spin and dephosphorylated with Antarctic phosphatase. The 3' construct was ligated using only

*Bam*HI as restriction enzyme. The correct orientation of the 3' insert was checked by digestion with *Pst*I. Restriction sites were located on the *kif3* gene at position 3704 bp and on the pET24b vector.

Kif5-353:

PCR was performed on the plasmid Kif5-476+pET24b. The purified PCR product was cloned directly into the pET24b expression system using *Nde*I and *Bam*HI as restriction enzymes.

Kif5-476:

The purified PCR product was cloned with blunt ends into the pBluescript II KS vector and the *Nde*I restriction site on position 1209 bp was mutated with a modifying oligonucleotide (5'-CTT GTT TAT AAT GGT ACA CTT TTA GCG TAT GGT CAA ACA GG-3'). The modified plasmid was ligated into the pET24b expression system using *Nde*I and *Hind*III as restriction sites.

GFP-fusion constructs:

The purified PCR products were cloned into the pA6PGFP-L-SSEB2 and the pDiscGFPSSSEB2, respectively, using *Sal*I and *Bam*HI as restriction sites. The full-length constructs was cloned in two steps: first the N-terminal part using *Sal*I and *Bam*HI, subsequently the C-terminal part using *Bam*HI as restriction site.

Citrine Kif3-342:

The purified PCR product was cloned directly into the pDiscCitrineSSEB2 expression system using *Nde*I and *Sal*I as restriction sites (Cai et al., 2007).

RFP Kif3-tail

The purified PCR product was cloned into the pBluescript II KS vector. The construct was subsequently ligated into the 339-3 Sal mRFPmars expression vector using *Sal*I and *Eco*RV as restriction sites.

2.3.16 Transformation of *Dictyostelium* cells

2.3.16.1 Electroporation

D. discoideum cells were grown to a density of $2-3 \times 10^6$ cells/ml, harvested and washed once in cold Soerensen buffer and twice in cold electroporation buffer. Cells were resuspended in cold electroporation buffer at a final density of 1×10^8 cells/ml, mixed with 15-30 μ g of plasmid DNA and transferred to a pre-chilled and sterile electroporation cuvette (distance between electrodes 4 mm). After two pulses (1.0 kV, 3 μ F) in an electroporation device (Gene pulser: Biorad, Hercules, CA, USA) cells were transferred to a sterile tissue culture dish for a 15 min recovery period at room temperature. After the addition of an $MgCl_2/CaCl_2$ solution (final concentration 1 mM each) cells were gently agitated for another 15 min at room temperature. Finally, cells

were resuspended in 25 ml HL-5c medium and distributed into a 24-well plate in case of blasticidin resistance being used. After a recovery period of 24 h, 4 µg/ml blasticidin S was added and the cells were incubated for 8-14 days until colonies of resistant cells appeared. In case of G418 resistance, cells were first incubated in liquid medium for 24 h and then plated on phosphate agar plates together with a dense solution of freshly grown *Klebsiella pneumoniae* cells. After 3-14 days incubation at 21°C feeding plaques appeared and transformants were lifted with a sterile pipette tip from the edges and transferred to a 24-well plate with HL-5c medium containing G418 (10 µg/ml) and a penicillin/streptomycin solution (Sigma).

2.3.16.2 Cloning of transformants

Transformants resulting from constructs containing the blasticidin gene were resuspended with a sterile pipette, a droplet of the cell suspension was transferred to a coverslip and cells were examined by immunofluorescence microscopy. If cells with the desired marker were found, different concentrations of the remaining cells were plated on SM agar plates together with a dense suspension of *K. pneumoniae* cells. After 3-14 days incubation at 21°C feeding plaques appeared and transformants were lifted with a sterile pipette tip from the edges and transferred to a 24-well plate with HL-5c medium containing blasticidin (10 µg/ml) and a penicillin/streptomycin solution (Sigma).

2.3.17 Southern blotting

For each sample 6 µg of genomic DNA from *D. discoideum* were prepared and digested with 40 U of enzyme in a volume of 250 µl. Another 40 U of enzyme were added after 3 h for the same incubation time. The digested DNA was extracted with phenol and chloroform and precipitated by ethanol. The pellet was dissolved in 15 µl loading buffer and heated shortly to 94°C.

Fragments were separated on a 0.8 % agarose gel for 30 min at 50 V and stained in ethidium bromide and documented. The gel was then incubated for 15 min in 0.25 M HCl and washed in H₂O. In order to denature the DNA the gel was incubated in 0.5 M NaOH and 1.5 M NaCl three times for 15 min and washed in H₂O subsequently. After neutralizing the denaturing agents with 1 M Tris/HCl pH 7.0 and 1.5 M NaCl for 15 min for a total of three times, the DNA was transferred in 10 x SSC buffer to a HybondN nylon membrane (GE Healthcare, München) by capillary force over night. The membrane was subsequently air dried and irradiated with UV for 1.5 min.

2.3.18 DiG hybridization

DNA probes were synthesized by PCR and marked with the “DIG DNA Markierungs- und Detektionssystem” (Boehringer Ingelheim, Biberach). For the PCR a 20 x dNTP mixture was supplemented with the same volume of 10 x DIG DNA marker mixture which resulted in the same dNTP concentration in the reaction. The marked probe was purified and eluted from an agarose gel.

Nylon filters containing immobilized DNA were pre-incubated with Easy Hyb solution (Boehringer Ingelheim) at 37°C for 1 h in a hybridization chamber. The DIG marked probe was added in a concentration not less than 50 ng per 100 cm² filter membrane and hybridized at 37°C over night (the concentration of the probe was estimated from agarose gels stained with ethidium bromide). Membranes were washed twice in high salt buffer for 5 min and twice in low salt buffer for 15 min at 65°C and subsequently equilibrated in maleic acid buffer for 5 min. Detection was carried out by an anti-DIG antibody coupled with alkaline phosphatase, diluted 1:5,000 in maleic acid buffer with 1 % blocking reagent (Boehringer Ingelheim). After an incubation time of 30-60 min 3 washing steps with maleic acid buffer, each lasting 10 min, washed out unbound antibodies. The probe was detected by CSPD-luminescence (Roche Diagnostics).

High salt buffer

2 x SSC, 0.1 % SDS

Low salt buffer

0.1 x SSC, 0.1 % SDS

Maleic acid buffer

100 mM maleic acid, 150 mM NaCl; pH 7.5

2.4 Biochemical methods

2.4.1 SDS-polyacrylamide gel electrophoresis

Proteins were separated on discontinuous SDS-polyacrylamide gels containing 10-12 % polyacrylamide (PAA). The gels were run in the “Multigel-Long-System” (Biometra, Göttingen) at 50-100 V. Samples and high molecular weight standard (Sigma) were mixed with Laemmli sample buffer, incubated at 95°C for 2 min and loaded onto the gel.

PAA solution

30 % acrylamide, 0.8 % bisacrylamide (Biorad)

Running buffer

25 mM Tris·HCl, 0.1 % SDS, 192 mM glycine

10 x buffer for stacking gel

500 mM Tris·HCl, pH 6.8, 0.4 % SDS

10 x buffer for separating gel

1.5 M Tris·HCl, pH 8.8, 0.4 % SDS

6 x Laemmli sample buffer

300 mM Tris-HCl, pH 6.8, 15 mM EDTA, 12 % SDS, 30 % glycerol, 15 % mercaptoethanol, 0.06 % bromphenol blue

2.4.2 Staining of SDS-gels

Gels were stained for 60 min in Coomassie staining solution, rinsed with ddH₂O and de-stained with 10 % acetic acid. Gels were photographed with a CCD camera (Eagle Eye System, Stratagene) or scanned (Epson 1200 Photo) for documentation.

Gels used for qualitative analysis were stained with the “Colloidal Blue Staining Kit” (Invitrogen) following the instructions of the manufacturer. Subsequently the gels were de-stained with water for 24 h and photographed with the Eagle Eye System prior to analysis.

Coomassie staining solution

7.5 % acetic acid, 50 % methanol, 0.25 % Coomassie Brilliant Blue R250 (Sigma)

2.4.3 Expression of kinesin constructs

A 200 ml pre-culture was inoculated with a freshly transformed single colony of *E. coli* BL21 CodonPlus(DE3)-RIL (Stratagene) containing the adequate vector and grown overnight at 37°C and at constant shaking at 220 rpm. This pre-culture was diluted into 5 l Erlenmeyer flasks containing 2 l TP-medium to an OD₆₀₀ of 0.02. Bacteria were grown with 2 ppm Antifoam (Sigma) at 22°C until the OD₆₀₀ of the culture reached 0.8 to 1.0. The culture was then chilled to 16°C in order to prevent the formation of protein clusters and 1 mM IPTG was added. The culture was incubated for at least 24 h at 16°C and constant shaking (220 rpm). Bacteria were harvested at 4°C and 3,500 rpm in a centrifuge (Beckman Coulter, Fullerton, CA, USA) and stored at -70°C.

2.4.4 Protein purification

2.4.4.1 Kif3-constructs

Kif3-protein constructs were purified in two steps: first by His-Tag selection with NiNTA then by gel filtration.

2.4.4.1.1 His-Tag selection

6-8 g of frozen BL21 CodonPlus(DE3)-RIL cells expressing the construct were resuspended in 3 volumes of lysis buffer. The suspension was sonicated (4 x 30 sec, output: 4, duty cycle: constant, Branson sonifier 250) and centrifuged (Beckman rotor 42.1: 42,000 rpm, 30 min, 4°C).

5 ml of NiNTA-Agarose suspension (QIAGEN) were incubated twice for 10 min at 4°C on a rolling device with 15 ml lysis buffer without ATP and imidazole. The NiNTA was

pelletized by centrifugation (500 rpm, 2 min, 4°C) and the supernatant discarded. The NiNTA pellet was incubated with the bacterial lysate for 1 h at 4°C on a rolling device. A column was poured and washed with at least 70 ml wash buffer until no protein was detectable by photometric absorption at E_{280} nm. The protein was eluted with 12 x 1 ml fractions of NiNTA-elution buffer. Fractions were tested in an ATPase assay and active fractions were pooled.

Lysis buffer

50 mM NaH_2PO_4 , 500 mM K-acetate, 10 mM imidazole, 2 mM MgCl_2 ; pH 7.5, 2 mM ATP, 10 mM β -mercaptoethanol, 0.5 μM Pefabloc (Roche Diagnostics), 1 x protease inhibitor (Pi), lysozyme, DNase I

Protease inhibitor (Pi)

1 mg/ml soybean trypsin inhibitor, 1 mg/ml TAME, 250 $\mu\text{g/ml}$ leupeptine, 100 $\mu\text{g/ml}$ pepstatine A, 100 $\mu\text{g/ml}$ aprotinin

Wash buffer

50 mM NaH_2PO_4 , 500 mM K-Acetate, 20 mM imidazole, 2 mM MgCl_2 ; pH 7.0, 1 mM ATP, 10 mM β -mercaptoethanol

NiNTA-elution buffer

50 mM NaH_2PO_4 , 500 mM K-Acetate, 160 mM imidazole, 2 mM MgCl_2 ; pH 7.0, 1 mM ATP, 10 mM β -mercaptoethanol

2.4.4.1.2 Gel filtration

In order to minimize the volume for the gel filtration the pooled fractions were concentrated via an Amicon Ultra centrifugal filter device (Millipore) with a nominal molecular weight exclusion limit of 10,000 or 50,000 depending on construct size. Centrifugation times at 4,000 g and 4°C in a Rotanta 460R centrifuge (Hettich, Tuttlingen) varied from 20 min for the Kif3-342 construct to 3 x 20 min for the Kif3-full-length construct.

A Sephadex G 1000 column was washed with at least 30 ml gel filtration buffer prior to adding the concentrated protein solution to the column with a 1.0 ml syringe. The flow rate was 0.2 ml/min. Protein was monitored by a UV monitor and recorded. 1.0 ml fractions were collected after a running time of 10 min. Subsequently 1 mM DTT was added to the sample. The active fractions were identified by ATPase assays. The purity of active fractions was checked by SDS-PAGE. Active and pure fractions were pooled, supplemented with 1/10 volume of glycerol, frozen in liquid nitrogen in small aliquots and stored at -70°C.

Gel filtration buffer

50 mM NaH_2PO_4 , 500 mM K-acetate, 2 mM MgCl_2 ; pH 7.0, 1 mM ATP, 10 mM β -mercaptoethanol, 1 mM DTT

2.4.4.2 Kif5 constructs

To select for active motor proteins, Kif5 constructs were purified via a microtubule binding and release step.

2.4.4.2.1 Microtubule affinity purification

5 g of frozen BL21 CodonPlus(DE3)-RIL cells expressing the construct were suspended in 15 ml lysis buffer. The suspension was sonified (4 x 30 sec, output: 4, duty cycle: constant, Branson sonifier 250) and spun clear of debris (Beckman rotor 42.1: 42,000 rpm, 30 min, 4°C). 20 µM taxol (paclitaxel, Invitrogen), 0.3 – 0.5 mg/ml taxol-stabilized microtubules, 0.2 mM AMP-PNP, and 5 U/ml apyrase were added to the supernatant and incubated for 30 min on a rolling device at room temperature. The kinesin-microtubule complexes were sedimented (Beckman rotor 42.1, 42,000 rpm, 30 min, 4°C) and the supernatant discarded. The pellet was washed once with AP100 containing 1 mM DTT and resuspended in 1 ml KCl buffer. The solution was spun through a sucrose cushion (40 % sucrose in AP100, 1 mM DTT, 10 µM taxol) to remove tubulin that did not polymerize (Optima rotor TLA 100.3, 80,000 rpm, 22°C, 10 min). The pellet was resuspended in 200 µl release buffer and incubated for 15 min at room temperature to ensure the complete release of active motors. Microtubules were sedimented (Optima rotor TLA 100.3, 80,000 rpm, 22°C). The release procedure was repeated once. Kinesin constructs in the release fractions were identified by SDS-PAGE and tested in ATPase assays. Small aliquots were supplemented with 1/10 volume of glycerol, frozen in liquid nitrogen, and stored at -70°C

AP100

100 mM PIPES·KOH, 2 mM MgCl₂, 1 mM EGTA; pH 6.8

Lysis buffer

AP100, 10µM ATP, 0.2 mM Pefabloc (Roche Diagnostics), 1 x Pi, 1 mM DTT, lysozyme, DNase I

KCl buffer

AP100, 50 mM KCl, 0.2 mM AMP-PNP, 10 µM taxol, 1 mM DTT

Release buffer

AP100, 300 mM K-acetate, 10 mM MgCl₂, 10 mM ATP, 20 µM taxol, 1 mM DTT, 0.5 mM EGTA

2.4.5 Purification of pig brain tubulin

Pig brain tubulin was purified in three successive steps of polymerization and depolymerization, followed by affinity chromatography. Fresh pig brains were obtained in the local slaughterhouse, immediately put on ice and separated from blood vessels and connective tissue. 700 g of brains were mixed with buffer A and homogenized in a pre-cooled warring blender (Braun, Kronberg) and centrifuged (Sorvall GSA-rotor:

13,000 rpm, 4°C, 70 min). The supernatant was supplied with 25 % glycerol and 2 mM ATP. To polymerize the tubulin, the mixture was incubated for 30 min in a water bath of 35°C. Microtubules were sedimented by ultracentrifugation (Beckman rotor Ti35: 35,000 rpm, 50 min, 32°C and Beckman rotor Ti45: 42,000 rpm, 45 min, 32°C). The pellets were resuspended in 100 ml buffer C and homogenized on ice in bounce homogenizers (Wheaton, Millville, NJ, USA). Microtubules were allowed to depolymerize on ice for 25 min and centrifuged again (Beckman rotor Ti42.1: 36,000 rpm, 30 min, 4°C). After addition of 2 mM ATP the supernatant was polymerized again (incubation for 30 min at 35°C) and centrifuged (Beckman rotor Ti42.1: 33,000 rpm, 45 min, 32°C). Microtubules were depolymerized once again by dissolving the pellet in 50-100 ml buffer B and homogenized for 25 min on ice. After centrifugation (Beckman rotor Ti42.1: 36,000 rpm, 30 min, 4°C) pellets were discarded and polymerization of the tubulin in the supernatant was induced with 10 % DMSO and 2 mM ATP (incubation for 30 min at 35°C). Microtubules were sedimented (Beckman rotor Ti42.1: 34,200 rpm, 45 min, 32°C) and resuspended in 10 ml buffer D, again homogenized and depolymerized on ice for 25 min. The supernatant of the final centrifugation step was loaded onto a phosphocellulose column with a peristaltic pump (150 ml of activated phosphocellulose suspension (P-11, Whatman) were packed into a column (Amersham-Pharmacia, now GE Healthcare, Little Chalfont, England) and equilibrated with 3 volumes of buffer D at 1 ml/min using the FPLC system (Amersham-Pharmacia). The column was washed with buffer D at a flow rate of 1 ml/min. Under the given conditions tubulin did not bind to the phosphocellulose material while microtubule associated proteins (MAPs) were retracted. The unbound protein was collected in 1.5 ml fractions and tubulin-containing fractions were identified with Bradford reagent (1 µl sample added to 400 µl H₂O and 100 µl Bradford reagent). Peak fractions were pooled, supplemented with 0.1 mM GTP and frozen in liquid nitrogen. Tubulin was stored at -70°C.

Buffer A

0.1 M PIPES·KOH, 2 mM EGTA, 1 mM MgSO₄, 1 mM DTT, 100 µM ATP

Buffer B

0.5 M PIPES·KOH, 2 mM EGTA, 1 mM MgSO₄, 1 mM DTT, 1 mM ATP

Buffer C

0.1 M PIPES·KOH, 2 mM EGTA, 1 mM MgSO₄, 1 mM DTT, 1 mM ATP

Buffer D

0.1 M PIPES·KOH, 2 mM EGTA, 1 mM MgSO₄, 1 mM DTT, 50 µM ATP

All buffers were adjusted to pH 6.9 at 4°C.

2.4.6 Determination of protein concentration

The protein concentration was determined with Bradford reagent (Biorad). For each measurement, a standard curve was measured using bovine serum albumin (BSA) as reference. The absorption at 630 nm was determined in a microplate reader (Dynatech MR 5000) and the protein concentration was calculated using the BSA standard as reference.

2.4.7 Polymerization of microtubules

Tubulin was thawed on ice and already polymerized tubulin removed by ultracentrifugation (Beckman rotor TLA 100.3: 80,000 rpm, 4°C, 10 min). The remaining tubulin in the supernatant was stabilized by the addition of 1 mM GTP (incubation for 10 min at 37°C) and polymerized by incubating for 20 min at 37°C. The addition of 20 µM taxol (paclitaxel, Molecular Probes) stabilized the microtubules. To remove unpolymerized tubulin, the microtubules were sedimented through a 40 % sucrose cushion, containing 20 µM taxol (Beckman rotor TLA 100.3: 80,000 rpm, 25°C, 10 min). The microtubule pellet was washed once with assay buffer containing 20 µM taxol and then resuspended in this buffer. The volume was adjusted to achieve a final concentration of about 100 µM tubulin heterodimers.

Microtubule concentrations were determined by measuring the absorption at 280 nm in a spectrophotometer. Microtubules were diluted 5-fold and 10-fold into the assay buffer containing 20 µM taxol. 10 µl of these solutions were mixed with 90 µl guanidinium·HCl (6.6 M) in order to denature the protein and expose the tryptophane residues. From the absorption of these mixtures the microtubule concentration was calculated according to the following equation:

$$C_{(\text{tubulin dimers})} [\mu\text{M}] = (E_{280} / 10.3) \cdot \text{dilution} [\mu\text{M}]$$

To obtain fluorescent microtubules for microscopic assays non-fluorescent tubulin heterodimers and tubulin dimers labeled with the fluorescent dye Atto 488 (Attotec,) were mixed in a ratio of 1:20 prior to a clear spin (Beckman Optima rotor TLA 100.3: 80,000 rpm, 4°C, 10 min). Polymerization was induced by the addition of GTP and taxol as described above.

2.4.8 Microtubule-stimulated ATPase activity

The microtubule-activated steady state ATPase rates were determined in a coupled enzymatic assay. In this assay the ATP turnover is coupled to the oxidation of NADH to NAD⁺ by the enzymes lactate dehydrogenase (LDH, Roche Diagnostics) and pyruvate kinase (PK, Roche Diagnostics). PK converts ADP to ATP, thus guaranteeing a constant ATP concentration during the reaction. The second substrate of PK, phosphoenolpyruvate (PEP, Sigma) is oxidized to pyruvate, a substrate of LDH. LDH reduces pyruvate to lactate and oxidizes its co-substrate, NADH (Sigma) to NAD⁺. The

rate of NADH oxidation was observed in the photometer at 340 nm (Kontron Uvicon 930, now Tresser Instruments, Groß-Zimmern).

The assay was performed in 12A25+ buffer at 22°C. The $K_{0.5(\text{MT})}$ was determined at saturating ATP concentrations (1 mM). The microtubule concentration was maintained at approximately 10 μM for titrations with ATP. The other substrates were supplied at saturating concentrations ($c_{(\text{PEP})} = 5 \text{ mM}$, $c_{(\text{NADH})} = 250 \mu\text{M}$). PK and LDH concentrations were 0.01 and 0.025 U/ μl , respectively. Microtubules were prepared as described in 2.4.7 and diluted in 12A25 with 20 μM taxol. Typically, the reaction was started with 1 μl kinesin. The mixture was quickly transferred into a 50 μl quartz cuvette (Hellma, Mülheim) and the decrease of extinction at 340 nm was monitored in the photometer for 1 min. The initial slope of the signal ($\Delta E/\text{min}$) was plotted against the corresponding microtubule concentration. Data points were fitted using a hyperbolic equation (Kaleidagraph software):

$$\Delta E = \Delta E_{\max} \cdot [\text{MT}] / ([\text{MT}] + K_{0.5(\text{MT})}) + B$$

yielding the maximal rate of the change of extinction ($\Delta E_{\max}/\text{min}$) and the microtubule concentration for half maximal activation ($K_{0.5(\text{MT})}$), and a background B. If the ATP concentration for half maximal activation was to be determined the fitting parameters were altered to:

$$\Delta E = \Delta E_{\max} \cdot [\text{ATP}] / ([\text{ATP}] + K_{0.5(\text{ATP})}) + B$$

The background signal (B) was typically below 0.1 % of the maximal rate.

Provided that the enzyme is supplied in excess, the generation of ADP and depletion of NADH are directly coupled, because the turnover rates of PK and LDH are much faster than kinesin. Thus, the maximal turnover per second can be determined via the law of Lambert-Beer:

$$E = \epsilon \cdot c \cdot d \Leftrightarrow E/t = (\epsilon \cdot c \cdot d)/t \Leftrightarrow V = c/t = (E/t) / (\epsilon \cdot d)$$

$$V_{\max} = (\Delta E_{\max} / 60 \text{ s}) / (d \cdot \epsilon)$$

ΔE_{\max} : maximal rate of NADH oxidation per minute

d: thickness of the cuvette (1 cm)

ϵ : extinction coefficient for NADH ($6.22 \text{ mM}^{-1} \cdot \text{cm}^{-1}$)

The maximal steady-state turnover rate k_{cat} corresponds to the maximal turnover rate of a single kinesin motor domain. The k_{cat} is derived by dividing the change of ATP concentration in time $\Delta[\text{ATP}]/\text{s}$ by the kinesin monomer concentration $[\text{kinesin}]$ in the assay:

$$k_{\text{cat}} = \Delta[\text{ATP}] / \text{s} \cdot [\text{kinesin}]$$

$[\text{kinesin}]$: concentration of kinesin polypeptide chains in the assay [g/l]
determined by Bradford assay

Hence, the k_{cat} value [1/s] is the maximal amount of ATP which is hydrolyzed by one kinesin head per second.

12A25 buffer

12.5 mM Aces·KOH; pH 6.8, 2 mM Mg-acetate, 25 mM K-acetate, 1 mM EGTA

2.4.9 Multiple motor gliding assay

Kinesin binds non-specifically with its tail on microscope coverslips while the motor region stays flexible. In the multiple motor gliding assay this feature is used to determine the protein's maximum velocity indirectly via the speed of single microtubules. 8 μl of a kinesin solution diluted in BRB80 with 10 % casein (v / v) was applied onto a coverslip (24 x 32 mm) flanked with two stripes of vacuum grease. After approximately 5 min of incubation in a wet chamber a smaller coverslip (18 x 18 mm) was stuck onto the vacuum grease stripes to seal the floating chamber. 37 μl of motility buffer containing 3 μl diluted and Atto 488 labeled microtubules, 3 μl oxygen-scavenger, and 1 μl ATP was subsequently flushed through the chamber.

Microtubule dilution: 1:100 in BRB80, 20 μM taxol, sheared by a 1 ml syringe

The velocity of the microtubules was observed in a TIRF microscope (Olympus, Hamburg) and recorded through a CCD-camera (C9100, Hamamatsu, Hamamatsu City, Japan), which took 500 single pictures with time intervals of 200 ms. The running length of single microtubules was determined using Olympus' cell[^]R software. Kinesin's velocity was then calculated by dividing running length by time span.

BRB80

80 mM PIPES·KOH, pH 6.8, 5 mM MgCl_2 , 1 mM EGTA

Motility buffer

10 mM MgCl_2 , 1 mg/ml casein, 20 μM taxol, 4.5 mg/ml glucose, 200 mM KAc, 1 mM DTT, in BRB80

Oxygen-scavenger

2.16 mg/ml glucose-oxidase (GOD), 0.36 mg/ml catalase, BRB80

2.4.10 Gliding of kinesin labeled with quantum dots

The photostability of quantum dot nanocrystals (Qdots) allows long-term imaging that would inactivate other types of fluorophores (Alivisatos et al., 2005; Michalet et al., 2005). Therefore Qdots (Qdot[®] 525 ITK[™] Streptavidin Conjugate Kit, 2 μM solution; Invitrogen) were chosen to label kinesin for gliding experiments. 4 pmol Qdots were added to 10-20 μM kinesin, BRB80 buffer was added to a total volume of 50 μl . After mixing by pipetting and incubation on ice for 5 min, 10 μl casein (10 mg/ml) were mixed to the solution in order to block unbound Qdots.

To obtain biotinylated fluorescent microtubules non-fluorescent tubulin heterodimers, tubulin dimers labeled with rhodamine, and 2 short chain and 1 long chain aliquot of biotinylated microtubules were mixed with 1 mM GTP prior to a clear spin (Beckman Optima rotor TLA 100.3: 80,000 rpm, 4°C, 5 min). Microtubules were polymerized at 35°C for 15 min and 20 μ M taxol was added before another incubation period of 15 min at 35°C. The solution was diluted 1:20 in BRB80 with 20 μ M taxol.

10 μ l of 0.33 mg/ml biotinamidocaproyl labeled BSA was flushed into a flow chamber (2.4.9) and incubated for 10 min. The flow chamber was then washed with 70 μ l non-fluorescent BSA solution. 10 μ l of 0.33 mg/ml streptavidin solution was flushed into the chamber, incubated for 10 min, and washed out with 70 μ l non-fluorescent BSA solution. 15 μ l of the biotinylated fluorescent microtubule dilution were flushed into the chamber and incubated for 5 min before washing with 70 μ l non-fluorescent BSA solution. Subsequently, 44.5 μ l of motility buffer were mixed with 2.5 μ l oxygen scavenger (2.4.9), 1 μ l ATP, and 2 μ l of kinesin labeled with Qdots and were flushed into the chamber.

The sample was placed on the TIRF microscope, microtubules were identified, and the gliding of the Qdot-kinesin-complexes recorded.

Biotinamidocaproyl labeled BSA solution

1 mg/ml in 1 x PBS, diluted 1:3 in BRB80

Streptavidin solution

1 mg/ml in 1 x PBS, diluted 1:3 in BRB80

Motility buffer

1 mg/ml casein, 4.5 mg/ml glucose, 200 mM KAc, 1 mM DTT, in BRB80

2.4.11 Purification of the Kif3-342 antibody

Purified Kif3-342 protein was blotted onto a nitrocellulose membrane and cut out with a scalpel. The membrane was saturated over night in NCD-buffer and 3 % fish-gelatin. The antiserum was diluted 1:1 in NCD buffer and incubated at least 3 hours. The membrane was washed 3 times in NCD buffer and the antibody was released by addition of 200 μ l glycine-HCl (100 mM; pH 2.5). The eluate was neutralized by 8 μ l 1 M Tris and stored at 4°C.

NCD buffer

100 mM Tris·HCl, 1.5 M NaCl, 0.02 % Tween20, 0.02 % NaN₃; pH 8.0

2.4.12 Western blots and immunostaining

Polyacrylamide gels were blotted with the semidry procedure using the buffer system described by Kyhse-Anderson (Kyhse-Anderson, 1984). The procedure was modified by the addition of 20 % methanol to all three buffers.

Blotting was carried out for one hour at 1 mA/cm^2 and blots were reversibly stained with 0.1 % Ponceau S (Sigma) in 5 % acetic acid prior to immunostaining. Marker bands were labeled on the blot before blocking in TBST, containing 3 % fish-gelatin. Incubation with the primary antibody diluted in TBST with 1 % fish-gelatin was carried out for 1 h at room temperature on a shaking device. Blots were then washed three times for 5 min each with TBST. The secondary antibody was coupled to alkaline phosphatase and also diluted in TBST with 3 % fish-gelatin (1:10,000). An incubation period of 45 min at room temperature was necessary. The blots were washed three times in TBST and once in TBS for 2 min each.

Color detection was carried out by 5 min incubation in AP reaction buffer, supplemented with 4.5 $\mu\text{l/ml}$ NBT (75 mg/ml stock solution in 70 % dimethylformamide) and 3.5 $\mu\text{l/ml}$ BCIP (50 mg/ml stock solution in 70 % dimethylformamide).

Alternatively, detection was carried out using the ECL-detection system (AppliChem, Darmstadt) according to the manufacturer's instructions. Gelatin was substituted by skim milk powder and secondary antibodies were coupled to peroxidase. X-ray films detected the luminescence.

TBST

20 mM Tris/HCl; pH 7.4, 150 mM NaCl, 0.05 % Tween-200

AP reaction buffer

100 mM Tris/HCl; pH 9.5, 100 mM NaCl, 50 mM MgCl_2

2.4.13 Determination of oligomerization state

To measure the native molecular weight of the kinesin constructs and thus assess how many polypeptide chains are assembled in one molecule the oligomerization state was measured by gel filtration and density gradient centrifugation.

Sedimentation coefficients $S_{W,20}$ were measured by sucrose density centrifugation. Layering 500 μl of 21 %, 18 %, 15 %, 11 %, 9 %, 7 %, and 5 % sucrose solution into an ultracentrifuge vial generated a sucrose gradient. Kinesin together with a set of standard proteins with a known $S_{W,20}$ (aldolase $S_{W,20} = 7.4$, BSA $S_{W,20} = 4.3$, ovalbumin $S_{W,20} = 3.6$, carboanhydrase $S_{W,20} = 3.2$) was diluted into a total volume of 300 μl buffer A to a final concentration of 0.2 mg/ml. The gradient was manually fractionated into 300 μl aliquots and analyzed by SDS-PAGE. The position of protein peaks in the gradient was identified by densitometric analysis using the NIH software ImageJ. The peak positions of the standard proteins were plotted against the corresponding $S_{W,20}$ values. Data were fitted by linear regression. The $S_{W,20}$ values of kinesin were calculated using the standard proteins as reference (Sigma plot software).

Stokes' radii (r_{Stokes}) were determined by gel filtration. A Sephadex 200 column (Amersham, GE Healthcare, Little Chalfont, England) was equilibrated with buffer A

and loaded with 500 µl of the protein solution (approx. 10 µM final concentration). Elution volumes of kinesin samples were compared with standard proteins (ferritin: $r_{\text{Stokes}} = 5.9$ nm, aldolase: $r_{\text{Stokes}} = 4.5$ nm, BSA: $r_{\text{Stokes}} = 3.5$ nm, carboanhydrase: $r_{\text{Stokes}} = 2.4$ nm, cytochrome c: $r_{\text{Stokes}} = 1.6$ nm; Roche Diagnostics Diagnostics and Sigma). Stokes' radii of kinesin proteins were determined from a plot of elution volumes versus Stokes' radii of the standard proteins (Andrews, 1970). The molecular weight was calculated according to the equation of Cantor and Schimmel (Cantor, 1980).

$$M_r = (S_{w,20} \cdot n_A \cdot 6\pi \cdot \eta \cdot r_{\text{stokes}}) / (1 - v \cdot \rho),$$

n_A is the Avogadro's number, η the viscosity (10^{-3} Nsm⁻²), v the specific volume of the sample (0.725 cm³/g), and ρ the density of the medium (1.0 g/cm³).

Buffer A

20 mM Na-phosphate, 500 mM K-acetate, 5 mM MgCl₂, 10 µM ATP, 1 mM DTT; pH 7.0

1 x PBS

140 mM NaCl, 2.7 mM KCl, 1.8 mM Na₂HPO₄; pH 7.4 (NaOH)

2.4.14 Isolation of mitochondria from *Dictyostelium* cells

GFP-marked *D. discoideum* Kif3 cells were grown in 1 l AX-medium to a density of 5×10^6 cells/ml. All subsequent steps were performed either on ice or in centrifuges cooled to 4°C.

The cell suspension was centrifuged for 5 min at 1,500 rpm and washed in a total volume of 20 ml phosphate buffer. This step was repeated twice. The cell pellet was suspended in 10 ml lysis buffer and vortexed for 1 min. The suspension was subsequently pressed through a Nucleopore filter (5 µm) and immediately centrifuged for 10 min at 3,000 rpm. The mitochondria remained in the supernatant. In order to sediment the mitochondria, the supernatant was centrifuged for 12 min at 17,000 g in a Sorvall SS34 rotor. The mitochondria were then resuspended in 20 ml SEM buffer and once more sedimented. The pellet was subsequently resuspended in 1 ml SEM buffer and its concentration determined via Bradford assay.

The following purification was performed using a sucrose gradient of 20, 30, 40, 50, and 60 % sucrose (Fluka) in 10 mM Mops-KOH pH 7.2 (w/w) with 1 mM EDTA, 1 mM PMSF, and protease inhibitor cocktail (PC). The gradient was centrifuged at 12,000 g in a TLS55 rotor for 15 min. The mitochondria accumulated between the 40 % and the 50 % sucrose phases and were concentrated by centrifugation in an Eppendorf cap at 12,000 g for 10 min. This pellet was rinsed in SEM buffer and centrifuged again. Subsequently it was resuspended in a small volume SEM buffer.

SEM buffer

250 mM sucrose, 10 mM Mops pH 7.2, 1 mM EDTA

Lysis buffer

SEM, 1 mM PMSF, protease inhibitor cocktail (PC)

Protease inhibitor cocktail (PC)

1 mM Pefabloc SC, 25 µg/ml leupeptin, 10 µg/ml tosylarginine methyl ester, 10 µg/ml soybean trypsin-inhibitor, 1 µg/ml aprotinin, 1 µg/ml pepstatin

2.4.15 Immunoprecipitation

Immunoprecipitation was performed basically as described by Hestermann (Hestermann and Graf, 2004). 200 ml of AX2 cells with a density of at least 5×10^6 cells/ml were washed in phosphate buffer and lysed in 8 x the volume of lysis buffer. The solution was pressed three times through a Nucleopore filter (5 µm). A cytosolic extract was obtained after centrifugation at 14,000 g for 15 min at 4°C. After incubation of the extract with varying amounts of antisera or purified antibodies for 1 h at 4°C, 20 µl of Protein G beads (50 % slurry pre-incubated with 0.1 % BSA in Tris buffered saline) were added for a further incubation for 1 h at 4°C in a rotator. The beads were washed 4 times with lysis buffer, resuspended with 30 µl of SDS sample buffer and subjected to SDS gel electrophoresis.

Lysis buffer

50 mM Hepes, 100 mM NaCl, 4 mM EGTA, 2 mM MgCl₂, 10 % sucrose, 0.3 % NP40, 1 x protease inhibitor cocktail (PC)

2.5 Cell biological methods

2.5.1 Immunofluorescence microscopy

Cells of a logarithmically growing *D. discoideum* culture were diluted to 5×10^5 cells/ml with HL5c medium. 150 µl of the cell suspension were pipetted onto a round coverslip and settled for 20 min. The cells were washed three times with Soerensen's phosphate buffer and fixed with the picric acid and paraformaldehyde method (Hagedorn et al., 2006).

After fixation the cells were washed 2 x 5 min with PBS/Glycin and 2 x 15 min with PBG. 150 µl of the primary antibody diluted in 1 x PBG were placed on the cells and incubated for at least three hours. Unbound antibodies were removed by washing 6 times for 5 min with PBG. The samples were then incubated for 1 hour with the diluted appropriate secondary antibody (Alexa 488-, Alexa 568- or Cy3-conjugates) and DAPI (1 µg/ml) to visualize nuclear and mitochondrial DNA. Subsequently the cells were washed 2 x 5 min with PBG and 3 x 5 min with PBS. Before the samples were embedded in Pro Long Antifade Kit (Molecular Probes), they were washed in H₂O.

Standard immunofluorescence microscopy preparations were viewed through a Zeiss Axiovert 200M microscope (Zeiss, Jena), equipped with a 100 x/1.3 objective and DAPI, rhodamine, and fluorescein filter sets. Images were recorded with an AxioCam Mrm camera on a computer running the program Axiovision 4.3.

PBS-glycine

1 x PBS; pH 7.4, 100 mM glycine

PBG

1 x PBS; pH 7.4, 0.5 % BSA, 0.045 % fish gelatine (Sigma G7765, 45 %), filtrated through sterile filter

2.5.2 Microtubule reorganization experiment

5×10^5 *D. discoideum* cells were centrifuged for 5 min at 4°C and washed twice with cold phosphate buffer. A 300 µl drop of the cell suspension was placed onto a round coverslip. The cells settled for 30 min. The phosphate buffer was carefully removed and replaced by a 10 µg/ml nocodazole-phosphate buffer solution. Cells incubated for 3 hours. A negative control incubated with the same amount of DMSO in phosphate buffer.

The DMSO-control and t_0 cells were fixated immediately; all other cells were washed with phosphate buffer and incubated for a certain time period (e.g. $t = 5, 10, 15, 20$ min) before they were also fixed with glutaraldehyde.

Glutaraldehyde-fixation

300 µl of a 0.5 % glutaraldehyde, 0.5 % Triton X-100 and 50 % PHEM-buffer solution were placed on the cells and incubated for 5 min. After 2 x 5 min washing with phosphate buffer a spatula tip of borohydride was given to the cells and incubated for 10 min. The cells were then washed for 5 and 10 min with phosphate buffer.

The primary antibody (in this case anti-tubulin, mAb YL1/2) was added and incubated for a minimum of 3 hours in a wet chamber at room temperature. The antibody was washed out in 5 steps with 1 x PBS, each step lasting 5 min.

The secondary antibody (goat-anti-rat Alexa 488) was diluted 1:1,000 in antibody dilution buffer and placed on the cells. It incubated for at least 1 hour at room temperature in a dark and wet chamber. The antibody was washed out with 1 x PBS in three steps, each lasting 5 min.

A 1:10,000 dilution of DAPI in 1 x PBS was added and incubated for 15 min. The cells were subsequently washed twice with 1 x PBS, shortly placed in H₂O, and embedded “face down” in Moviol.

PHEM-buffer

60 mM PIPES, 25 mM HEPES, 10 mM EGTA, 2 mM MgCl₂; pH 6.9

Antibody dilution buffer

1 x PBS, 0.1 % BSA, 0.1 % Na-azid

Moviol

120 mg/ml polyvinylalcohol 4-88, 30 % glycerole, 0.2 M Tris-HCl; pH 8.8

2.5.3 Phylogenetic analysis

Phylogenetic analysis was performed using 13 Kinesin-1 protein sequences that were chosen to represent diverse eukaryotic taxa, including plants (*Arabidopsis thaliana*, *Oryza sativa japonica cultivar*), fungi (*N. crassa*, *Ustilago maydis*, *Schizosaccharomyces pombe*, *Yarrowia lipolytica*, *Candida albicans*), protozoa (*D. discoideum*, *Cryptosporidium hominis*), and animals (*Homo sapiens*, *Drosophila melanogaster*, *Danio rerio*, *Caenorhabditis elegans*). The kinesin-13 sequence from *Xenopus laevis* was used as an out-group to root the tree. All sequences were downloaded from the NCBI Refseq database. Sequences were aligned using clustalW (v. 1.83) (Thompson et al., 1997) and refined with rascal (Thompson et al., 2003) using three iterations. A phylogenetic tree was constructed using MrBayes (v. 3.12) (Ronquist and Huelsenbeck, 2003) with the following settings: 50,000 generations, 4 chains, sample trees collected every 50 generations, and 250 sample trees as burn-in. In addition, a neighbor-joining (NJ) tree was constructed using the neighbor-joining algorithm (Saitou and Nei, 1987) as implemented within ClustalX with 1000 bootstrap replicates (taken from Roehlk et al., submitted 2007).

3 Results

3.1 *D. discoideum* kinesin Kif3

3.1.1 Phylogenetic analysis

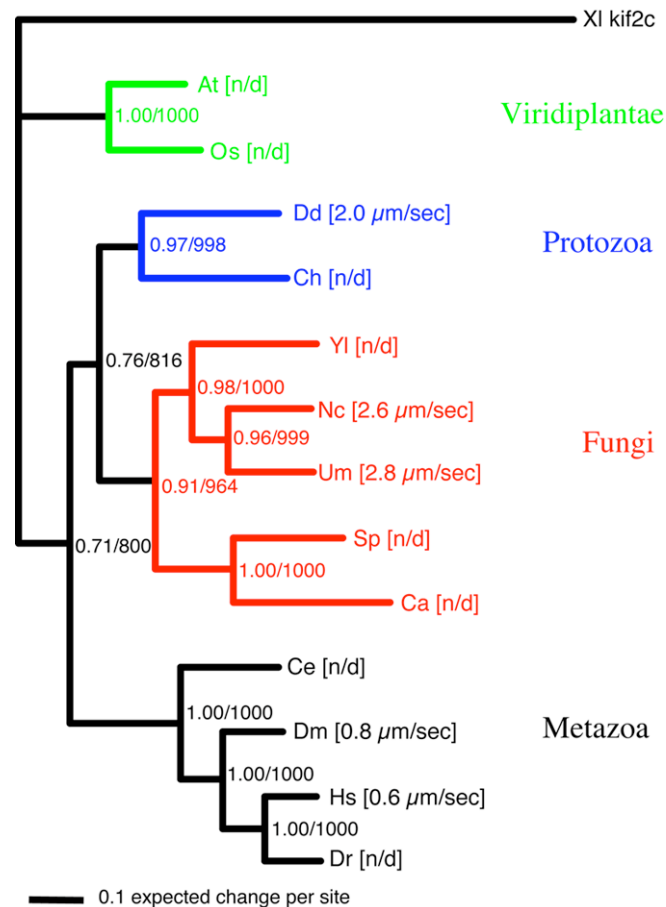
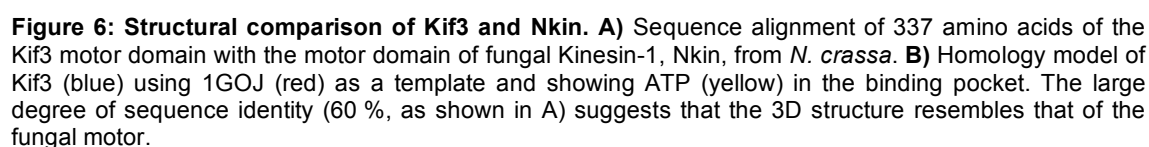


Figure 5: Phylogenetic analysis of Kif3 and 12 other kinesin-1 protein sequences. Sequences represent diverse eukaryotic taxa, including plants [At: *Arabidopsis thaliana* (gene access number: 30695816), Os: *Oryza sativa* japonica cultivar (50940525)], fungi [Nc: *Neurospora crassa* (Steinberg and Schliwa, 1996) (32419873), Um: *Ustilago maydis* (Wedlich-Soldner et al., 2002) (71020269), Sp: *Schizosaccharomyces pombe* (6502956), Yl: *Yarrowia lipolytica* (50543606), Ca: *Candida albicans* (68479181)], protozoa [Dd: *Dictyostelium discoideum* (66813336), Ch: *Cryptosporidium hominis* (67592791)], and animals [Hs: *Homo sapiens* (Malik et al., 1994) (45446749), Dm: *Drosophila melanogaster* (Hancock and Howard, 1998) (17136240), Dr: *Danio rerio* (68365994), Ce: *Caenorhabditis elegans* (17555418)]. The kinesin-13 sequence from XI: *Xenopus laevis* (13959688) was used as an out-group to root the tree. Published velocities corresponding to each kinesin are shown (n/d = not determined) (Roehl et al., submitted 2007).

The close relationship (60 % identity and 80 % similarity) to *Neurospora crassa*'s kinesin Nkin gave reason to model Kif3's motor domain based on the structure of Nkin (1GOJ), using Swiss Model as protein structure homology-modeling server (Guex and Peitsch, 1997; Schwede et al., 2003). Figure 6 shows the structure of the Kif3 motor domain compared with the motor domain of Nkin.



Two different constructs were created for homologous recombination using the pLPBLP [floxed Bsr] system (Faix et al., 2004) as described in 2.3.14. One construct replaced the first 95 amino acids of the motor protein's head with the Bsr-cassette; the other one disrupted the *kif3* gene between amino acids 113 and 436. Both constructs

were transformed at least eight times into *D. discoideum* AX2 cells. Blasticidin resistant clones were checked by PCR with primers inside the Blasticidin cassette and outside the introduced construct on the *kif3* gene. However, occasionally emerging resistant cells turned out to be false positive. Both constructs failed to establish a *kif3*-null cell line.

3.1.3 Expression and purification of Kif3 constructs

Three different His-tagged constructs were expressed in *E. coli* and purified as described in 2.3.15 and in 2.4.4. The shortest construct Kif3-342 (aa 1-342) consisted of the head domain and partial neck. The truncated kinesin Kif3-592 (aa 1-592) comprised the motor domain, neck and partial stalk. The full-length version Kif3 (aa 1-1194) included all amino acids of the protein (Figure 7 D).

The expression and purity of the kinesin constructs were confirmed by SDS-PAGE (Figure 7 A-C). The purity was nearly 90 %. The molecular mass of each construct was estimated from the gels: 40 kDa for Kif3-342 and 68 kDa for Kif3-592 in agreement with the values calculated from the amino acid sequences. The Kif3-full-length construct appeared at 160 kDa, roughly 20 % larger than calculated. A similar discrepancy has been observed in experiments involving *D. discoideum* extracts (Klopfenstein et al., 2002), indicating an aberrant mobility in the SDS gel.

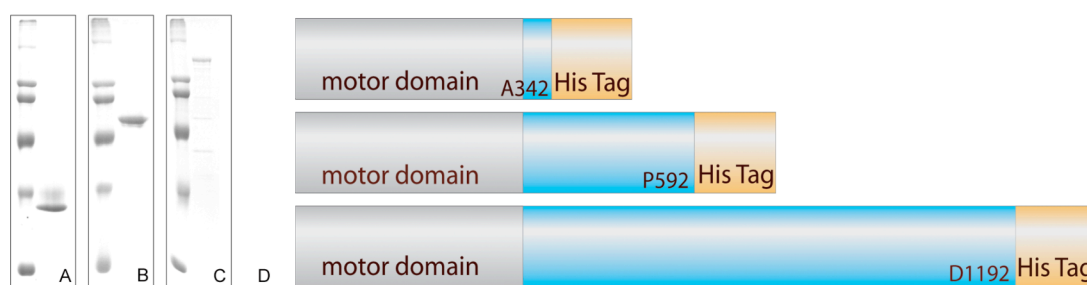


Figure 7: A-C) SDS-PAGE after purification. A: Kif3-342; B: Kif3-592; C: Kif3-full length. High molecular weight ladder: 29, 45, 66, 97.4, 116, 205 kDa. **D) Structure of Kif3 constructs.** Top: head construct Kif3-342, middle: truncated Kif3-592, bottom: Kif3-full-length. Letters and numbers indicate the last amino acid from the *D. discoideum* gene in the construct. A His-Tag as indicated was added C-terminally to each construct.

3.1.4 Oligomerization states

As only two-headed Kinesin-1 motors are known to possess processive motility (Hancock and Howard, 1998), the dimerization states of all three constructs were analyzed. The hydrodynamic behavior using velocity sedimentation through a sucrose gradient and gel filtration was performed twice with each of the constructs. The average S values and Stokes' radii are shown in Table 3. The molecular weight calculations using the equation of Cantor and Schimmel as described in 2.4.13 (Cantor, 1980) proved that the constructs Kif3-592 and Kif3-full-length are in a dimerized state, while

Kif3-342 is a monomer. All constructs were tested for their microtubule dependent steady-state ATPase-activities and microtubule gliding velocities in multiple motor gliding assays.

Table 3: Oligomerization states of Kif3-constructs.

Construct	r (Stokes) [nm]	$S_{w,20}$ [1S = 10^{-13} s]	Derived mass [kDa]	Predicted mass [kDa]	Oligomerization state
Kif3-342	2.36	3.69	35.9	40.0	monomer
Kif3-592	4.51	6.13	114.3	68.0	dimer
Kif3-full-length	5.48	10.60	240.0	131.0	dimer

Stokes' radii are given in nm. The derived mass matches the predicted mass for monomeric constructs. For dimers, the derived mass is doubled compared to the predicted mass. The calculated masses differ from the expected masses within a tolerable range due to the method of analysis.

3.1.5 Microtubule-stimulated ATPase activity

The steady-state ATPase activity was determined for all Kif3 constructs using a coupled enzymatic assay as described in 2.4.8 (Hackney, 1994). As kinesins are ATP-dependent, microtubule-activated enzymes, the ATPase rates were measured as a function of concentrations of both microtubules and ATP. The resulting hyperbolic plots were analyzed with the Michaelis-Menten equation. The resulting maximal turnover rate per kinesin head represents the k_{cat} value. The calculated $K_{0.5(MT)}$ represents the microtubule concentration that leads to half maximal activity of the kinesin. Although it corresponds to the K_M of Michaelis-Menten enzymes the $K_{0.5(MT)}$ is much lower than expected. The explanation for this discrepancy lies in the processivity of the kinesin. A processive molecular motor binds to the microtubule and stays attached for many steps. The catalytic cycle for an individual head not only includes ATP hydrolysis, but also conformational changes, movement, and re-attachment to the microtubule. During these phases the enzymatic ATPase activity is not the rate-limiting step. The implicit assumption of Michaelis-Menten kinetics that steps after substrate binding do not limit the rate does not apply.

The ATP turnover of the monomeric Kif3-342 occurred at a rate of $k_{cat} = 144.4 \text{ s}^{-1} \pm 5.9$ ($n = 2$ independent preparations), for the dimers Kif3-592 and Kif3-full-length $60.5 \text{ s}^{-1} \pm 1.6$ and $45.9 \text{ s}^{-1} \pm 2.4$, respectively. The half-maximal activation for microtubules $K_{0.5(MT)}$ was $0.29 \text{ } \mu\text{M}$ (polymerized tubulin concentration) for Kif3-342, $0.304 \text{ } \mu\text{M}$ for Kif3-592, and $2.15 \text{ } \mu\text{M}$ for Kif3-full-length. Figure 8 shows example traces of ATPase turnover for all three Kif3-constructs.

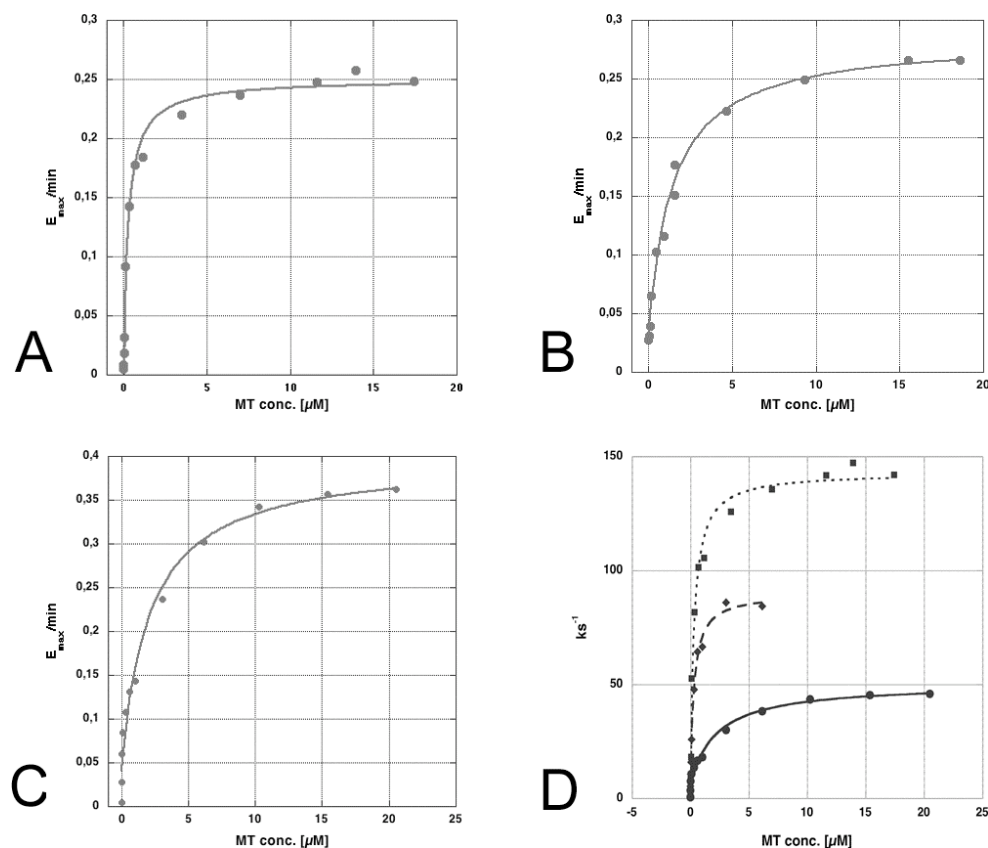


Figure 8: Kif3 ATPase assays with varying microtubule concentrations. A: Kif3-342 (head construct). B: Kif3-592 (truncated Kif3). C: Kif3-full-length. D: ATPase turnover of Kif3-constructs (solid line, round dots: Kif3-full-length; interrupted line, diamonds: Kif3-592; dotted line, squares: Kif3-342). The $K_{0.5(MT)}$ of the monomer Kif3-342 is much lower and the turnover rate k higher than the values for the dimeric constructs.

In order to find optimal conditions for enzymatic ATPase assays the ionic strength of the buffer was varied. The optimal activity of the dimeric Kif3-592 construct was reached between 100 and 300 mM potassium acetate with a k_{cat} of around 60 s^{-1} and a $K_{0.5(MT)}$ of 0.3 μM as shown in Figure 9. The motor protein was more sensitive to potassium chloride (optimum at 100 mM with k_{cat} of 47.6 s^{-1} and a $K_{0.5(MT)}$ of 0.55 μM) with a decreasing activity with more than 200 mM KCl and to sodium chloride (optimum at 50 mM with a $K_{0.5(MT)}$ of 0.87 μM) with a decrease in activity exceeding 50 mM NaCl (data not shown).

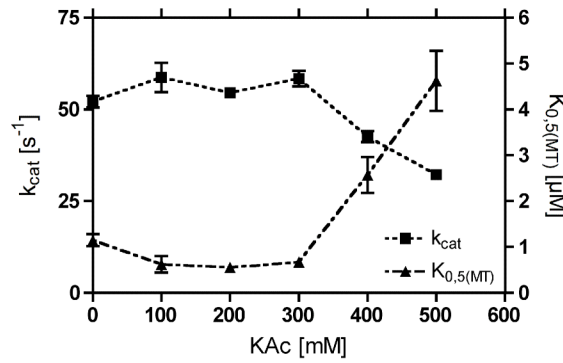


Figure 9: Dependence of Kif3-592 ATPase on ionic strength. The graph shows the dependence of the microtubule-activated ATP turnover k_{cat} and the half maximal activity concentration $K_{0.5(MT)}$ on ionic strength. ATP turnover rate and $K_{0.5(MT)}$ values show optimal activity at concentrations between 100 and 300 mM K-acetate. Activity decreases with concentrations exceeding 300 mM.

The temperature dependence of the Kif3-592 and -full-length protein was tested in ATPase assays, revealing an optimum at 27°C for both constructs (Figure 10). The values for Kif3-592 at 17°C and Kif3-full-length at 32°C were excluded due to unsaturated ATPase conditions, indicated by large error-bars for the $K_{0.5(MT)}$ values as shown in the graphs.

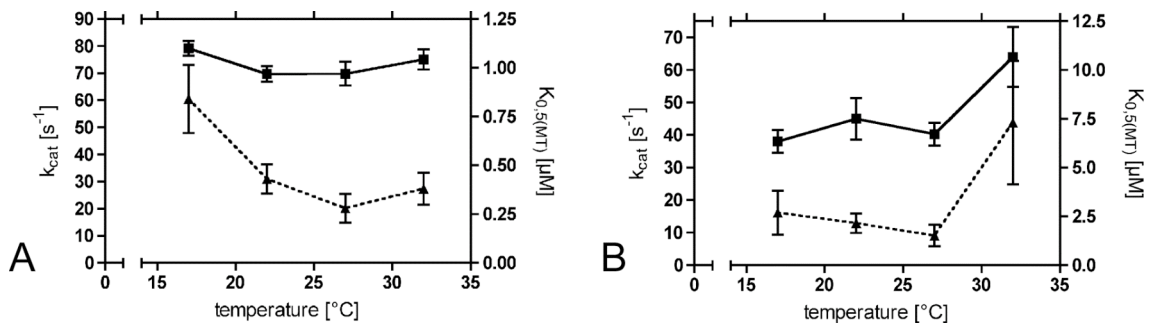


Figure 10: Temperature dependence of ATPase assays. k_{cat} solid line, squares; $K_{0.5(MT)}$ dotted line, triangles. Kif3-constructs were tested for ATPase activity at varying temperatures. **A)** Truncated Kif3-592. **B)** Kif3-full-length.

The apparent bimolecular binding rate $k_{bi(ATP)}$ contains implicit information on the processivity of an enzyme. In particular, the ratio of the apparent second-order constant $k_{bi(ATP)} = k_{cat}/K_{0.5(MT)}$ from the steady-state assays and the measured binding rate k_{bi} indicates the number of ATPase cycles induced by one productive diffusional encounter of kinesin and microtubule. The theoretical limit for the diffusional association between a kinesin motor and an individual tubulin subunit within a microtubule is approximately $30 \mu M^{-1}s^{-1}$ (Hackney, 1995). The apparent association rate between kinesin and microtubule $k_{bi(ATP)}$ yielded $198 \mu M^{-1}s^{-1}$ for the truncated construct Kif3-592 (see also Table 5).

3.1.6 Motility

The motility of the Kif3-592 and the Kif3-full-length constructs was tested in a microscopic gliding assay using a TIRF-microscope. The motor proteins bound unspecific to coverslips and without additional factors. As observed in the enzymatic assays, motility strongly depended on ionic-strength as shown in Figure 11. The maximum velocity in an inverted motility assay (moving microtubules on fixed motors) was reached at 200 mM K-acetate and was $1.77 \mu\text{ms}^{-1} \pm 0.01$ for Kif3-592 (mean \pm s.e.m.; 2 independent preparations; $n = 147$) and $1.96 \mu\text{ms}^{-1} \pm 0.01$ for Kif3-full-length (2 independent preparations; $n = 120$). Below this concentration the velocity was slower and more heterogeneous, and above it, less microtubule binding was observed. Therefore, this concentration was used as standard for all subsequent gliding experiments with the Kif3 proteins (Figure 11 A). A processive gliding assay with Kif3-342 was not expected due to the monomeric structure of this short construct. In the assay microtubules did not bind to Kif3-342 motors, neither with nor without addition of K-acetate, or by substituting ATP with AMP-PNP.

A temperature optimum for Kif3-592's gliding-velocity was observed at 27°C with $V_{\text{gld}} = 2.29 \mu\text{ms}^{-1} \pm 0.14$. Kif3-full-length was still active at higher temperatures and reached its maximum of $2.87 \mu\text{ms}^{-1} \pm 0.13$ at 32°C . A standard temperature of 22°C was kept to match the standard conditions (Figure 11 B).

The velocity of Kif3-full-length fluorescently labeled with Quantum Dot beads (Seitz and Surrey, 2006) was similar to that in the inverted assay ($2.17 \mu\text{ms}^{-1} \pm 0.18$; $n = 18$).

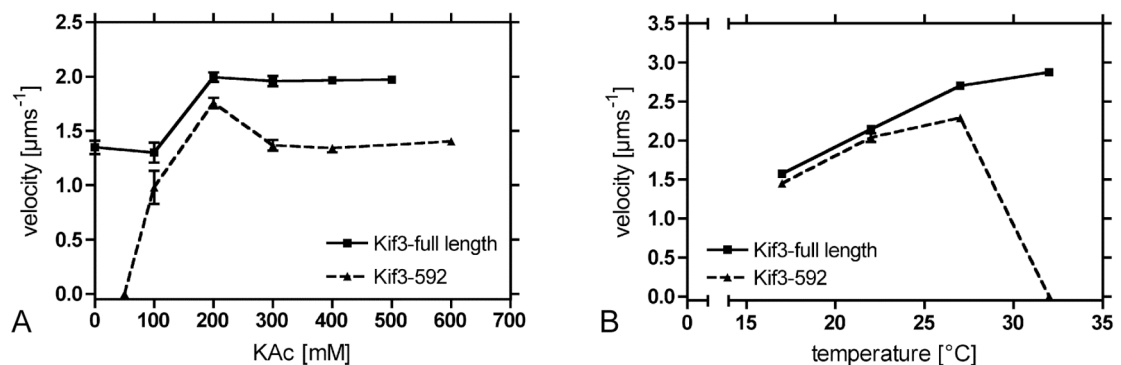


Figure 11: Temperature and ionic dependence of gliding velocities. A) KAc-dependence of motility. A maximum gliding velocity at 200 mM KAc was detected for Kif3-full-length and for Kif3-592. Both constructs revealed stable gliding velocities at KAc concentrations exceeding 500 and 600 mM respectively. **B)** A temperature dependent increase in gliding velocity for Kif3-full-length was observed, while Kif3-592 reached a maximum velocity at 27°C and was inactive at 32°C .

3.1.6.1 Single molecule gliding assay

The Kif3-full-length motor protein was diluted in a microscopic gliding assay to the point of single-motor attachment. Almost two thirds of the moving microtubules

(64.4 %, n = 59) moved shorter than their own length, indicating that single-molecule-gliding took place. Pivoting of the microtubules was not observed.

3.1.7 Duty ratio of Kif3-constructs

To determine the duty ratio r of Kif3 as a measure of a motor protein's dwell time on the filament relative to the duration of the complete catalytic cycle, the ratio of $K_{0.5(ATP)}$ in the ATPase- and gliding-assays was calculated for Kif3-592 and Kif3-full-length (Howard, 2001). The ratio for Kif3-592 resulted in $r = 0.306$ and for Kif3-full-length in $r = 0.414$, implying that the motor spent more than one third of the time bound to the microtubule (Table 4). Although this value is lower than the 50 % expected for processive motors in the Howard model, the value indicates enzymatic processivity because not all simplifications made in the model do actually apply in reality.

Table 4: Duty ratio r of Kif3-592 and Kif3-full-length.

	$K_{0.5(ATP)}$ (ATPase)	$K_{0.5(ATP)}$ (gliding assay)	Ratio r
Kif3-592	$266.7 \pm 6.0 \mu\text{M}$	$870.8 \pm 15.4 \mu\text{M}$	0.306
Kif3-full-length	$295.51 \pm 3.5 \mu\text{M}$	$713.36 \pm 8.5 \mu\text{M}$	0.414

3.1.8 Summary of Kif3's biochemical properties

Table 5 summarizes the averaged measured and calculated biochemical properties of all three Kif3-constructs. The microtubule gliding velocity of Kif3-342 was not determined (= n/d) due to its monomeric structure.

Table 5: Biochemical properties of Kif3-constructs.

	k_{cat} [s^{-1}]	$K_{0.5(MT)}$ [μM]	$k_{\text{cat}}/K_{0.5(MT)}$ [$\mu\text{M}^{-1}\text{s}^{-1}$]	$K_{0.5(ATP)}$ [μM]	velocity [μms^{-1}]
Kif3-342	144.4 ± 0.05	0.290 ± 0.046	497.93	0.146 ± 0.045	n/d
Kif3-592	60.5 ± 0.01	0.304 ± 0.031	198.88	0.267 ± 0.060	1.77 ± 0.01
Kif3-full-length	45.9 ± 0.05	2.146 ± 0.503	21.39	0.296 ± 0.035	1.96 ± 0.01

3.1.9 Kif3 GFP-fusion proteins and immunofluorescence

To investigate the cellular function of Kif3, GFP-tagged versions were constructed and introduced ectopically into *D. discoideum*. Constructs expressing GFP-Kif3 from the strong actin6 promoter (Graf et al., 2003) or the similarly strong discoidin promoter (Daunderer and Graf, 2002) revealed a cytoplasmic localization with strong local

accumulations (Figure 12). The staining pattern was most reminiscent to ER but no suitable antibody was available for co-staining. GFP-Kif3 did not co-localize with F-actin (as Kif5, described below).

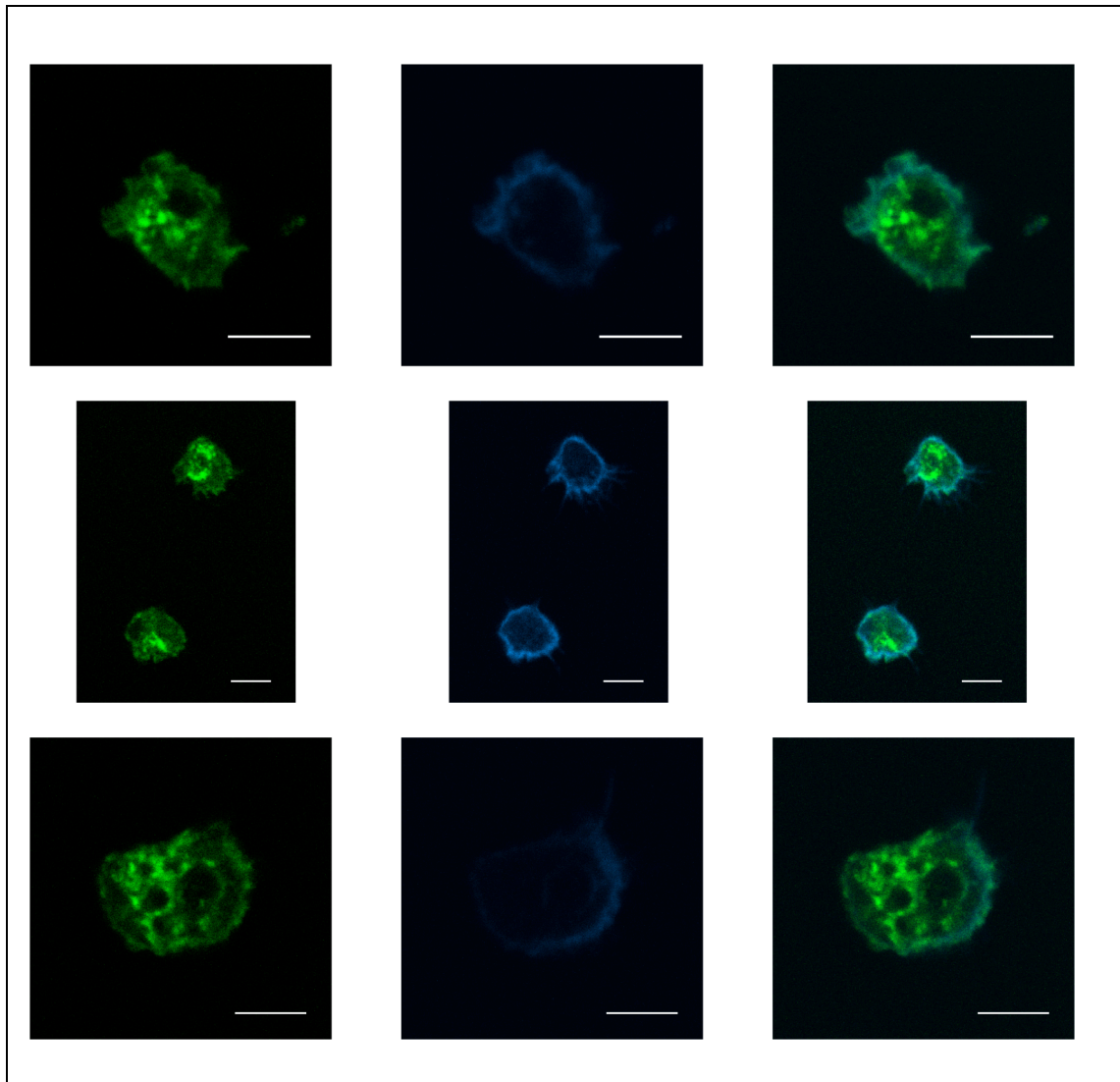


Figure 12: Kif3-full-length GFP-fusion protein. Three examples of *D. discoideum* cells expressing GFP-Kif3 and stained with phalloidin 635 show a cytoplasmic localization of GFP-Kif3 in a pattern reminiscent of ER. A co-localization with F-actin as shown for Kif5 by Iwai (Iwai et al., 2004) was not detected. Left column: GFP-fusion protein; middle column: phalloidin-Alexa635 antibody staining; right column: merged pictures. Single slices of confocal microscopy images; picric acid fixation. Scale bar 5 μ m.

To find out which region of the Kif3 protein determines its intracellular localization an RFP-expression vector expressing the Kif3-tail (amino acids Q569 to D1192) was transformed into *D. discoideum* cells expressing the Kif3-342 protein fused to citrine (Cai et al., 2007) (Figure 13). The overlap of both stains was small, suggesting independent localization of the fusion proteins. The citrine-Kif3-342 motor domain localized in a spotty cytoplasmic pattern, comparable to that observed with antisera in

Kif3-342 over-expressing strains. The stained parts did not show the ER-like shape of the full-length GFP-motor. In contrast, the RFP-tail construct localized to cytoplasmic structures resembling those observed in antibody staining, but sometimes also to cytoplasmic cups. These observations indicate that Kif3's tail domain is responsible for proper cellular localization. A strain expressing only the RFP-tail construct could not be generated, possibly due to the competition of the overexpressing RFP-tail with endogenous kinesin.

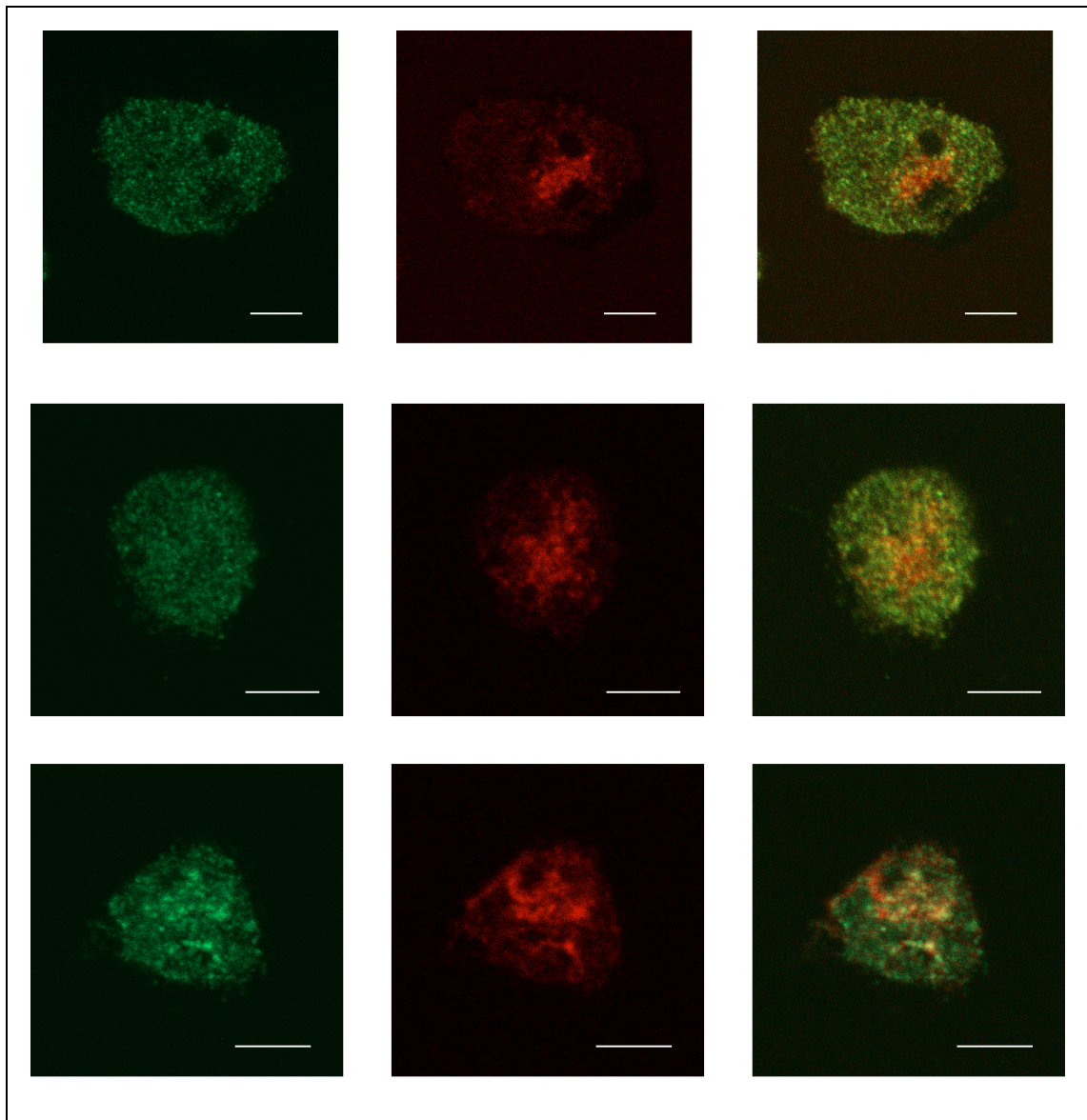


Figure 13: Cells expressing Kif3-342 citrine-fusion protein were transformed with an RFP-expression vector containing the Kif3-tail. Left column: Kif3-342 citrine-fusion; middle column: Kif3-tail RFP-fusion; right column: merged pictures. Kif3-342 Citrine and Kif3-tail RFP-constructs did not co-localize. Single slices of confocal microscopy images; picric acid fixation. Scale bar 5 μm.

To find out whether the areas of higher intensity reflect the endoplasmic reticulum, the strain was co-stained with a monoclonal calnexin-antibody (Muller-Taubenberger et al., 2001). Unlike expected from the staining pattern of GFP-Kif3 immunofluorescence microscopy did not show co-localization of GFP-Kif3 and calnexin, arguing against the endoplasmic reticulum as a cellular cargo of Kif3 (Figure 14).

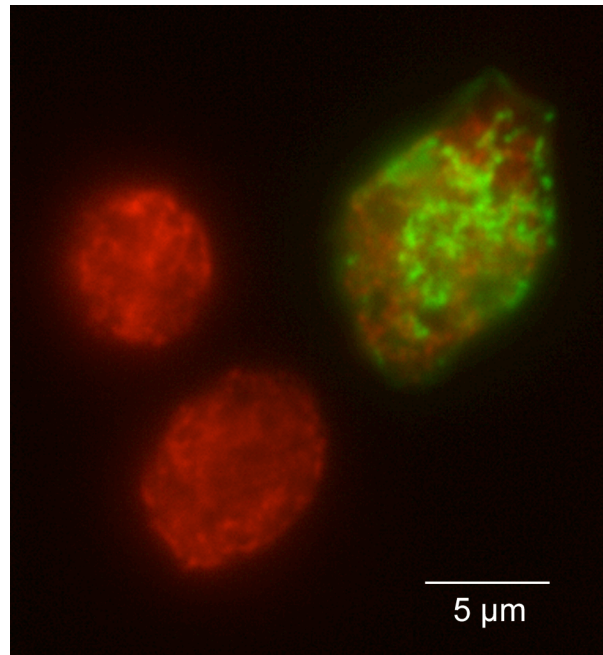


Figure 14: N-terminal GFP-fusion protein of Kif3-full-length. Co-staining of endoplasmic reticulum with Calnexin 270-390-2 monoclonal antibody and Alexa 568 secondary antibodies (picric acid fixation). Cells on the left are GFP-negative controls; cell on the upper right shows strong GFP-expression. No co-localization of Kif3 with the endoplasmic reticulum was observed. Single slice of confocal microscopy images; picric acid fixation. Scale bar 5 μ m.

Similarly, co-staining with mitochondria did not show co-localization. To this end, a *D. discoideum* strain with GFP-tagged mitochondria (DMIF-1 GFP) was stained with a polyclonal antibody against Kif3-342, which was obtained from rabbits injected with the Kif3-342 construct and affinity purified using a blot strip (2.4.11). In a Western blot, the purified serum reacted with Kif3 and two other bands of lower molecular weight. These bands were possibly other *D. discoideum* kinesins, degradation products of Kif3, or completely unrelated. The indirect immunofluorescence with this polyclonal antiserum did not show co-localization with GFP-mitochondria, suggesting that Kif3 is not associated with mitochondria (Figure 15). However, the distribution of Kif3 differed strongly from that observed in microscopy of GFP-Kif3 (Figure 12).

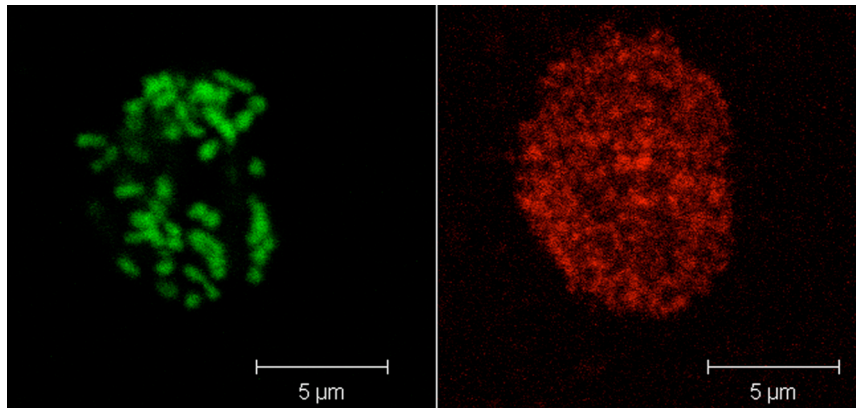


Figure 15: Immunostaining of DMIF1-GFP-marked (localizes to mitochondria (2.2.1)) AX2 cells with Kif3-342 polyclonal antibody and Cy-3 secondary antibody. Kif3 is distributed throughout the cell (red fluorescence, right), but shows no co-localization with GFP-labeled mitochondria (left). Single slice of confocal microscopy images; picric acid fixation. Scale bar 5 µm.

3.1.10 Western Blots

Western Blotting was performed using the purified Kif3-342 polyclonal antibody. AX2 wild type and GFPKif3 cell-lysates were separated on a SDS-gel and blotted onto a membrane, which was subsequently incubated with the Kif3-342 antibody. Figure 16 shows the blot with 5 distinct bands in the AX2 lane and with two more distinct bands in the GFPKif3 lane. The kinesin Kif3 is expected to run at 160 kDa, bands of that particular size can be found in both cell-lysates. As expected, an additional band approximately 30 kDa larger can be found in the GFPKif3 lysate.

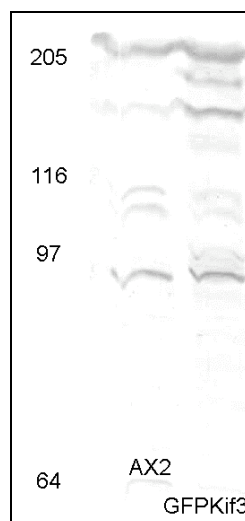


Figure 16: Western Blot with Kif3-342 antibody. AX2 wild type and GFP-Kif3 cell lysates were separated on a SDS-gel and blotted onto a membrane, which was subsequently incubated with the Kif3-342 antibody. Marker sizes are indicated by numbers; size in kDa.

In order to check mitochondria isolated from GFPKif3 cells for bound kinesin, they were analyzed by Western blotting. The blot with mitochondria and supernatants from the isolation process was stained with antibodies against GFP (anti-GFP), tubulin (mAb YL1/2), and porin from mitochondria (anti-porin 70-100-1). A co-localization of tubulin or GFP from Kif3 with the mitochondria could not be observed. The tubulin and kinesin-GFP were detected only in the supernatants.

3.1.11 Immunoprecipitation

An immunoprecipitation with AX2 cell-lysate and the Kif3 antiserum and the purified antibody showed three distinct bands on SDS-gels. The bands were isolated and analyzed by mass spectrometry in the Zentrallabor für Proteinanalytik, LMU Munich. Myosin and actin precipitated with the serum and the purified antibody, while the immunoglobulin γ 1 region was also found in the anti-serum precipitate. Kinesin was not detected.

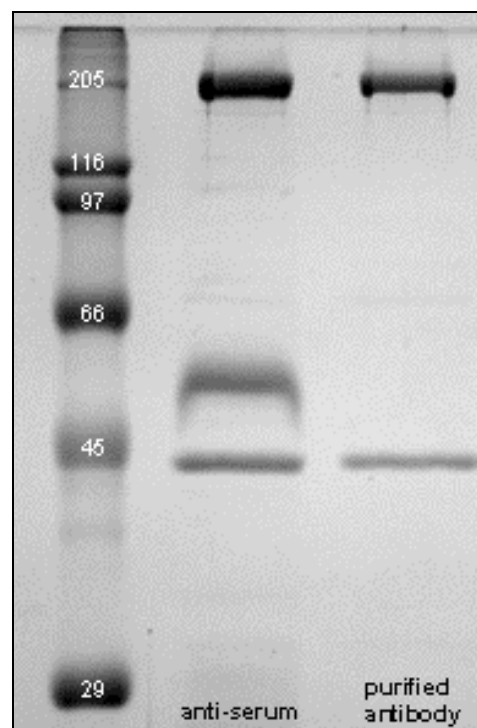


Figure 17: Immunoprecipitation. AX2 cell-lysate was incubated with the Kif3-342 antiserum and the purified antibody. Myosin (at 205 kDa) and actin (just under 45 kDa) precipitated in both cases. The immunoglobulin γ 1 region was only detected in the anti-serum precipitate. Kinesin was not detected.

3.2 *D. discoideum* kinesin Kif5

The second conventional kinesin in *D. discoideum* is Kif5. An initial characterization was published by a Japanese group while the work on this project was still in progress (Iwai et al., 2004). Nevertheless the work on Kif5 was continued, the gene was disrupted and the phenotype characterized. A GFP-fusion protein revealed Kif5's localization in *D. discoideum* cells. The publication failed to reveal Kif5's biochemical properties; therefore its ATPase and gliding velocity were determined.

3.2.1 Kif5-null mutants

A knockout cell line was established by homologous recombination using the pLPBLP [floxed Bsr] system (Faix et al., 2004) (Figure 18A). PCR and Southern Blot analysis confirmed the knockout (Figure 18B).

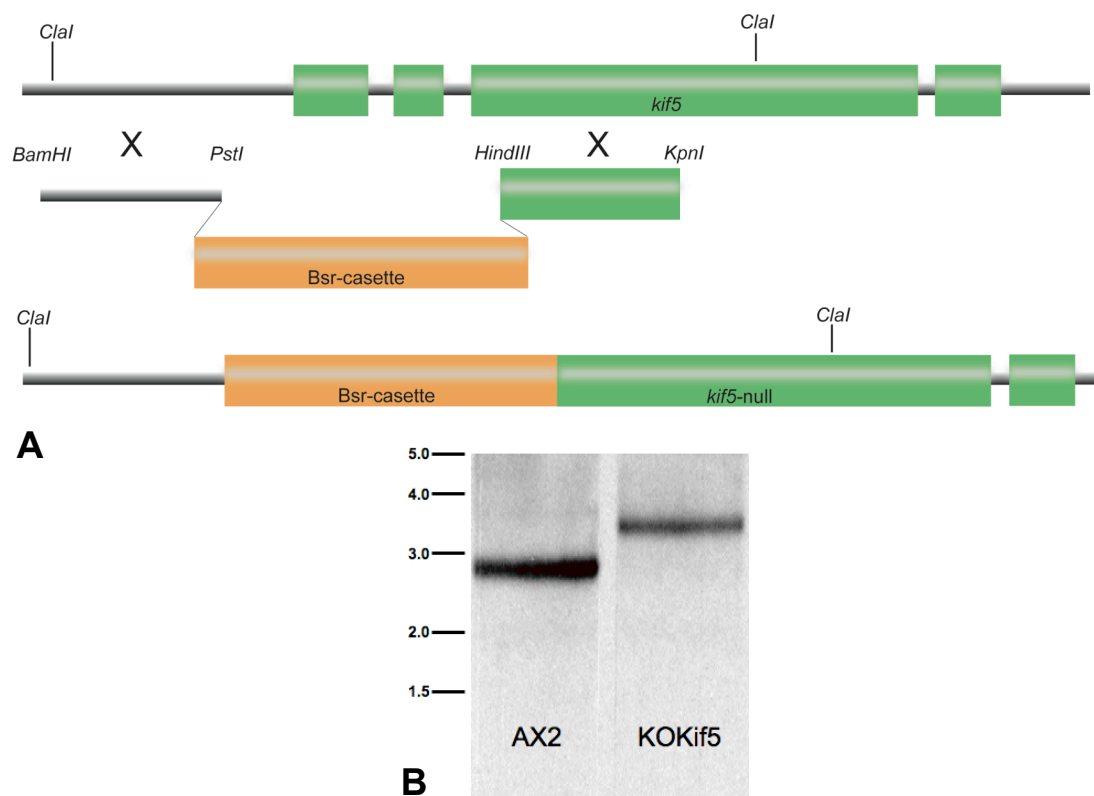


Figure 18: A) Disruption of the *kif5* gene. A schematic representation of the *kif5* gene. The construct used for the disruption of the *kif5* gene is drawn below. Bsr = Blastocidin S resistance gene. Restriction sites used for cloning were introduced in the primers. *Clal* restriction sites were used for Southern Blot confirmation of the gene disruption. **B) Southern Blot analysis of the *kif5* gene disruption.** Ladder marker in base pairs. Wild type AX2 and KOKif5 DNA was isolated from cells and digested with *Clal*. Southern Blot revealed expected sizes of 2,908 bp for AX2 and 3,428 bp for KOKif5. Sizes differ due to the introduction of the 1,350 bp Bsr-cassette.

The Kif5-null mutants showed no apparent phenotype. However, growth curves with submerged *D. discoideum* cultures in cell culture flasks showed a reduced speed of growth of Kif5-null cells compared to wild type AX2 cells (Figure 19). Interestingly, no significant differences between wild type and null-mutants were observed in shaking cultures.

To test the hypothesis of Kif5 being an anchor for actin to microtubules (Iwai et al., 2004), the microtubules of Kif5-null and AX2 control cells were temporarily depolymerized by applying 10 $\mu\text{g/ml}$ nocodazole to the cells. The nocodazole was washed out and microtubules reorganized for a determined period of time prior to fixation. A deviation compared to the wild type AX2 cells in the time needed for reorganizing the microtubule network could not be observed for the Kif5-null cells. Both cell lines reorganized their microtubule network within 10 minutes (Figure 20).

Further phenotyping such as slug-motility assays and growth experiments on *Klebsiella* plates revealed no indication on the *in vivo* function. As already indicated and published (Iwai et al., 2004), Kif5-null cells do not show a specific phenotype.

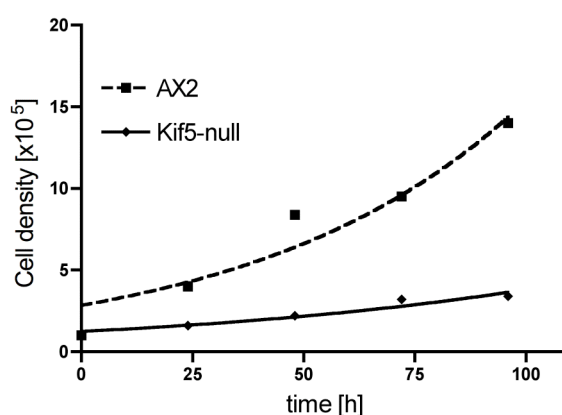


Figure 19: Growth curve of submerged *D. discoideum* cultures. Averaged values from two independent experiments. Kif5-null cells display a reduced growth speed. Both cell lines started at the same density of 1×10^5 cells. Regression curves were calculated and might not fit to the point of origin.

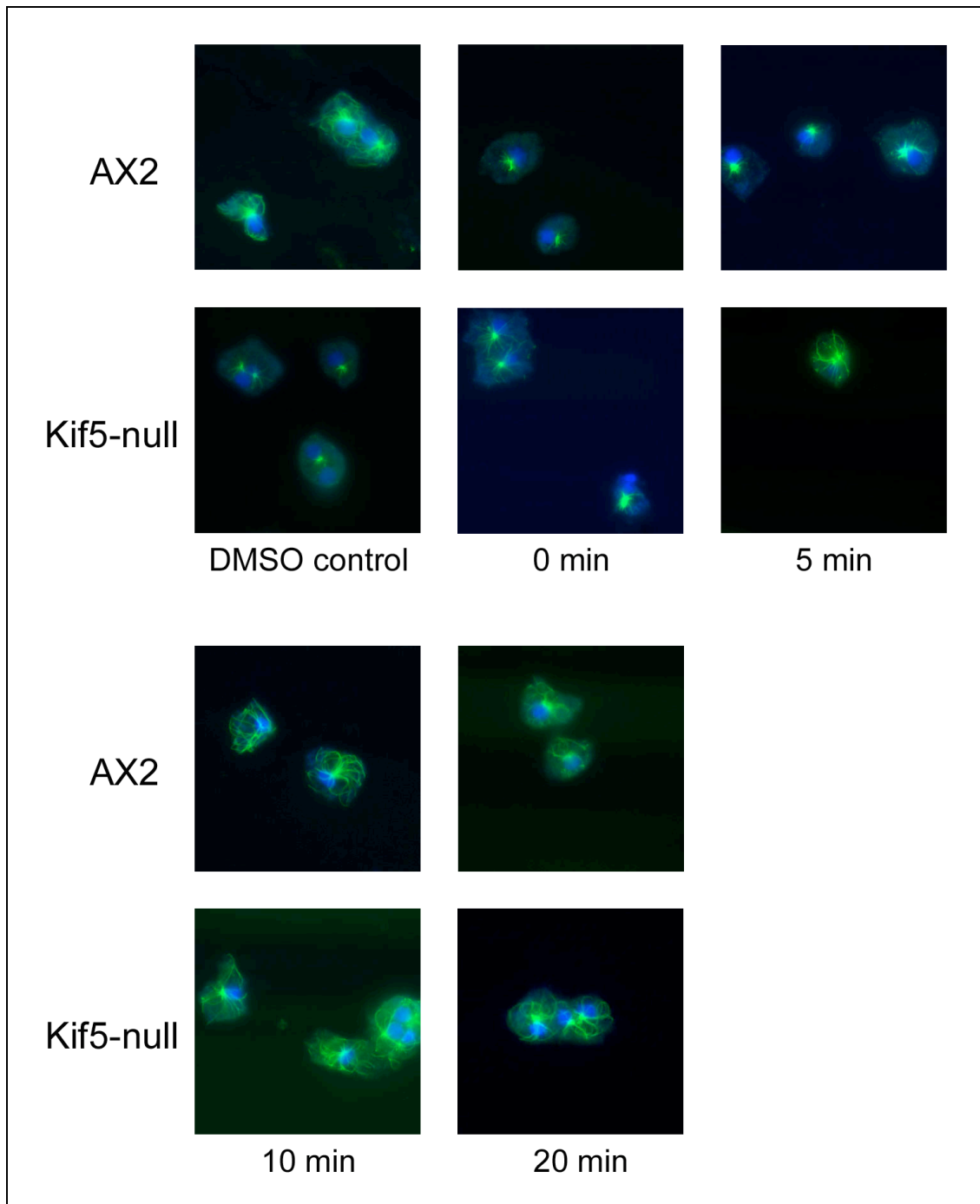


Figure 20: Microtubule reorganization in Kif5-null cells. Nocodazole depolymerized the microtubules. Nocodazole was washed out and cells incubated in phosphate buffer for 0, 5, 10, and 20 minutes prior to fixation. DMSO control on the very left without nocodazole. No deviation from wild type AX2 cells (top row) was observed for Kif5-null cells (bottom row). Staining with Anti-Tubulin mAb YL1/2 antibody and goat-anti-rat Alexa 488 secondary antibody; DAPI. Glutaraldehyde fixation.

3.2.2 Expression and purification of Kif5 constructs

Two different constructs were expressed in *E. coli* and purified by microtubule binding as described in 2.4.4.2.1. The shortest construct Kif5-353 (aa 1-353) consisted of the

head domain and a partial neck and expressed a His-Tag at the C-terminal end. The truncated kinesin Kif3-476 (aa 1-476) comprised the motor domain, the neck and a partial stalk (Figure 21).



Figure 21: Structure of Kif5 constructs. Top: head construct Kif5-353, bottom: truncated Kif5-476, Letters and numbers indicate the last amino acid from the *D. discoideum* gene in the construct. KHC stands for kinesin head complex. A His-Tag as indicated was added C-terminally to Kif5-353.

3.2.3 Microtubule-stimulated ATPase activity

The steady-state ATPase activity was determined for all Kif5 constructs using a coupled enzymatic assay as described in Materials & Methods (Hackney, 1994). A detailed description of the theory of ATPase assays is given in 3.1.5.

An exact determination of the k_{cat} values was hampered due to a consistent co-purification of *E. coli* proteins with the Kif5 constructs. Figure 22 shows two ATPase assays with varying microtubule concentrations for both Kif5-constructs.

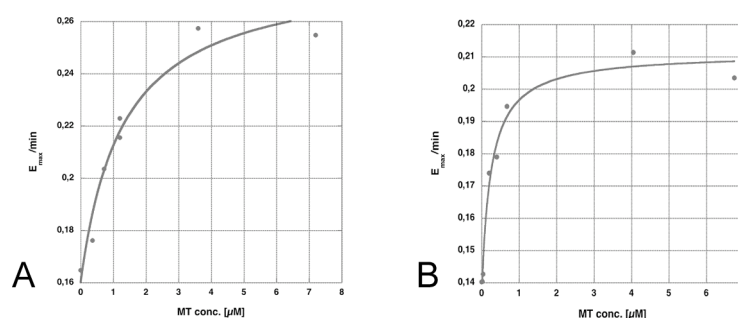


Figure 22: Kif5 ATPase assays with varying microtubule concentrations. A: Kif5-353 (head construct). B: Kif5-476 (truncated Kif5).

3.2.4 Motility

The motility of the Kif5-353 and Kif5-476 constructs was tested in a microscopic gliding assay using a TIRF-microscope. The gliding velocity for both constructs was below the detection limit. A binding of microtubules to Kif5-353 could not be observed. Microtubules bound to the motor protein Kif5-476 without additional salt. After

addition of 200 mM K-acetate to the assay buffer microtubules did not attach to Kif5-476 motors. In contrast to the experiments with Kif3 protein constructs, extra K-acetate kept microtubules from attaching to the motor protein Kif5-476.

3.2.5 Kif5 GFP-fusion protein

N-terminal GFP-fusion proteins, comprising the full-length Kif5 gene, were detected in the entire cell, but also predominantly localized in the cell's cortex (Figure 23). These results confirm the findings of Iwai et al., who also showed that Kif5 co-localizes with actin (Iwai et al., 2004).

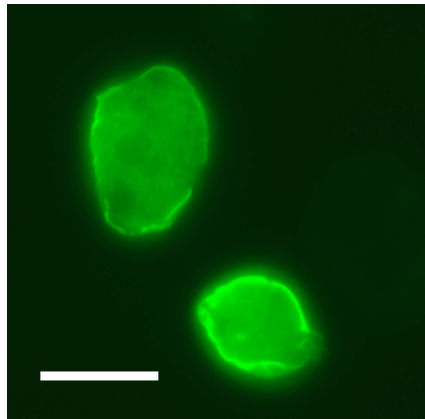


Figure 23: Kif5 GFP-fusion protein. Strong GFP signals in the cell's peripheries (picric acid fixation). Scale bar 10 μ m.

4 Discussion

Two kinesins represent the superfamily of Kinesin-1 (formerly conventional kinesins) in *D. discoideum*. Although up to three kinesins were grouped to the Kinesin-1 family (Kollmar and Glockner, 2003; Wickstead and Gull, 2006), only two of them carry a characteristic motor domain typical for conventional kinesins: Kif3 and Kif5. In this study both kinesins were characterized using biochemical, molecular biology, and cell biology methods.

4.1 *D. discoideum* Kif3

4.1.1 Biochemical *in vitro* properties

Kif3 is a motor protein that is able to move microtubules *in vitro*. Various assays in this work have shown that this conventional kinesin is a processive motor. The fact that in a microtubule-gliding assay under the lowest possible coating densities almost two thirds of the microtubules did not move further than their lengths strongly suggests that they were transported by single motor-molecules. Pivoting was rare under these conditions, indicating a stiff linkage between coverslip surface and the motor head. Indirect kinetic evidence stated below supports this view.

The high velocity of about $2.0 \mu\text{ms}^{-1}$ already strongly implies processive catalytic cycles of the enzyme if compared with other conventional kinesins from various organisms (see Figure 5). Furthermore, the high apparent association rate between kinesin and microtubule $k_{\text{bi(ATP)}}$ of almost $200 \mu\text{M}^{-1}\text{s}^{-1}$ for the truncated construct Kif3-592 suggests that Kif3 hydrolyzes several ATP molecules per microtubule encounter. The lower value of $21 \mu\text{M}^{-1}\text{s}^{-1}$ for the Kif3-full-length construct can be attributed to inhibiting structures possibly formed by tail regions of the full-length protein that are absent or less distinct in the truncated motors. Dimeric kinesins that do not bind cargo have been shown to be enzymatically inactivated (Hackney et al., 1992). Soluble kinesin was less active in a microtubule-stimulated ATPase assay than kinesin attached to beads (Jiang and Sheetz, 1995). Other researcher's results indicate that tail-motor interactions may mediate the inhibition of non-cargo-bound kinesin ATPase activity (Hackney et al., 1992; Hirokawa et al., 1989), explaining the discrepancy observed in these experiments.

The high value of $k_{\text{bi(ATP)}} = \text{almost } 500 \mu\text{M}^{-1}\text{s}^{-1}$ for Kif3-342 does not support the discussion about Kif3's processivity simply because its short structure prevents dimerization and therefore a processive catalysis. A gliding velocity for this short construct could not be determined; it lacked the elements from the stalk region that are necessary for non-specific binding to the coverslip. Substituting ATP with AMP-PNP in the microtubule gliding assay revealed no microtubule binding. When the assay buffer was flushed into the assay chamber, the motor proteins were probably rinsed out. Its

high microtubule induced ATPase activity is a strong argument against a functional defect of the motor protein.

Kif3-342's high $k_{bi(ATP)}$ may derive from a strong binding of the monomer to the microtubule due to the lack of a proper release mechanism (Jiang and Hackney, 1997). Although the real bimolecular association rate was not measured, the values for Kif3-592 are roughly ten-fold above the theoretical limit (Hackney, 1995), but at the same time do not quite reach the level reported for Nkin (Kallipolitou et al., 2001). On the other hand, the $k_{bi(ATP)}$ values were obtained under high ionic strength conditions, which usually diminish kinesin-microtubule interactions.

The duty ratio r defines the time fraction of the catalytic cycle a motor spends in the strongly filament-bound state. The ratio of $K_{0.5(ATP)}$ measured in a steady-state ATPase assay and in a multiple motor gliding assay is a reasonable estimate for r with the $K_{0.5(ATP)}$ of the gliding assay reflecting the situation in which half of the molecules "wait" for ATP in the microtubule-bound state, whereas the $K_{0.5(ATP)}$ in the steady-state ATPase results from intermediates of the entire cycle, including the unattached states (Howard, 2001). The duty ratios showed that the Kif3-592 construct stayed attached to the microtubule for at least one third of the catalytic cycle time and that the Kif3-full-length construct was attached for an even longer time period (40 % of the cycle). Although the duty ratios of Kif3-592 and -full-length were lower than 50 % and thus below the theoretical prediction for processive enzymes, they were far above the typical ratio for non-processive motors (Adio et al., 2006a; Howard, 2001). The discrepancy between the measured duty ratios and the theoretical value may be due to simplifications in the concept, which assumes that the $K_{0.5(ATP)}$ in gliding assays is determined only during the phase where kinesin is bound to the microtubule (Howard, 2001). If $K_{0.5(ATP)}$ and $K_{d(ATP)}$ deviate because of kinetic steps after microtubule detachment, this assumption is not true any longer (Fersht, 1999).

The decreasing ATPase activity but stable gliding velocity with potassium-acetate concentrations exceeding 300 mM might be an intrinsic consequence of the nature of the assays. Multiple motor gliding assays select for functional motor proteins, which dominate the assay while a significant portion of the motors is already thermally denatured, while in ATPase assays all motor proteins are detected simultaneously, and therefore a decrease in activity is inevitably measurable as soon as a moiety of enzymes displays a lower metabolic rate.

Due to the nature of processive stepping – two heads of a kinesin motor protein work hand-over-hand, alternating in microtubule attachment and ATP hydrolysis (Asbury, 2005) – and in agreement with animal and fungal kinesins, the monomer Kif3-342 possesses a faster ATPase than the dimeric constructs Kif3-592 and Kif3-full-length (144 versus 61 and 46 s^{-1}). For fungal kinesins k_{cat} values of 260 and around 70 s^{-1} have been reported for monomeric and dimeric constructs, respectively (Kallipolitou et al., 2001); for human kinesins 80 vs. 40 s^{-1} (Ma and Taylor, 1997). The average velocity in gliding assays of Kif3 under physiological conditions (around 2.0 μms^{-1}) showed a

higher similarity to the velocity of fungal Nkin ($2.6 \mu\text{ms}^{-1}$) (Kirchner et al., 1999) than to animal kinesins ($0.5 \mu\text{ms}^{-1}$) (Shimizu et al., 2000). The velocity of Kif3-full-length labeled with Quantum Dot beads ($2.17 \mu\text{ms}^{-1}$) was similar to that in the inverted assay and confirmed the evaluated speeds.

The most remarkable difference between Kif3 and Nkin was the strong dependence on high ionic strengths of the *D. discoideum* motor. The cytoplasm of *D. discoideum* does not contain unusually high salt concentrations, and therefore it is unknown whether this has a physiological significance. Possibly, the motors were purified in a repressed, folded state and high salt concentrations were necessary to relieve the inhibition (Hackney and Stock, 2000). The intramolecular ionic interactions involved in Kif3, however, have to be much stronger than reported for *Drosophila* or *Neurospora* kinesins (Seiler et al., 2000; Stock et al., 2003), and for kinesins of different nature.

Although the truncated motor Kif3-592 showed a higher ATPase rate than Kif3-full-length, the gliding assay revealed a higher velocity for the full-length construct. As for the $k_{\text{bi(ATP)}}$, tail-motor interactions may have mediated the inhibition of non-cargo-bound kinesin ATPase activity for Kif3-full-length, but only to a certain extent for the truncated Kif3-592 construct. Furthermore, it is assumed that the binding of the kinesin tail to the coverslip in gliding assays simulates cargo binding and therefore prevents a possible tail-motor inhibition, resulting in an unhindered gliding activity (Adio et al., 2006b; Coy et al., 1999; Yonekura et al., 2006).

In general, chemical reactions proceed faster at higher temperatures; kinesins are no exception to this rule. It has been shown that the gliding velocity of microtubules bound to kinesins increases to a certain point with an increase in temperature (Bohm et al., 2000). The question came up whether Kif3 is optimized for *D. discoideum*'s natural habitat temperatures. The increasing k_{cat} of Kif3-full-length revealed a temperature dependence of activity in ATPase assays, but not as strong as expected and described for other kinesins (Bohm et al., 2000; Mazumdar and Cross, 1998) and not according to Arrhenius exponential. Nonetheless, a maximum activity for the k_{cat} could be detected at 27°C , supported by the low $K_{0.5(\text{MT})}$ at the same temperature (Figure 10).

A more dramatic effect was observed in microtubule-gliding assays. The Kif3-full-length motor increased its velocity by approximately 50 % (from $2.0 \mu\text{ms}^{-1}$ at 22°C to almost $3.0 \mu\text{ms}^{-1}$ at 32°C), while the truncated construct Kif3-592 also increased its velocity but was inactive at temperatures exceeding 27°C . The truncated structure of Kif3-592 possibly reduced its sensibility towards outer influences. The broad spectrum of activity of Kif3-full-length shows that it functions at suboptimal temperatures in *D. discoideum*, with the ability to increase its speed by another 50 %.

4.1.2 Cellular localization and function of Kif3

Prior experiments indicated an involvement of Kif3 in vesicle transport (Pollock et al., 1999). In the Pollock experiments *D. discoideum* cells lacked one of two identified molecular motors - kinesin Unc104 - the microtubule plus-end-directed organelle

transport was not completely suppressed. It was assumed that Kif3 produced the remainder of the movement (Pollock et al., 1999). However, the nature of the transported vesicles remained unclear.

The close similarity to Nkin led to the assumption that *D. discoideum*'s Kif3 might also be involved in microtubule-dependent mitochondrial transport like its counterparts in *N. crassa* (Fuchs and Westermann, 2005), in mammalian cells, and in *Drosophila* (Khodjakov et al., 1998; Nangaku et al., 1994; Pereira et al., 1997; Tanaka et al., 1998). In order to test this hypothesis, mitochondria from GFPKif3 cells were isolated, lysed and denatured, separated by SDS gel electrophoresis, blotted, and stained with antibodies against tubulin, GFP, and mitochondrial porin. The antibody staining revealed no co-localization of mitochondria with any of the other tested proteins. Tubulin and GFP were found in supernatants from the isolation process, indicating that the method of isolation was too harsh and possibly disrupted the mitochondrial membrane; whereupon membrane associated proteins were set free.

A GFPKif3-fusion protein and immunostaining also showed no association with mitochondria or the endoplasmic reticulum during the vegetative stages of *D. discoideum*. By excluding the mentioned involvements in mitochondria transport and with the ER, lysosomes are the most likely cargo candidates. Methods for specifically labeling and isolating lysosomes from *D. discoideum* cells are published (Aubry, 2006; Rodriguez-Paris et al., 1993), but involve a special breakage method that has direct and deep repercussions on the quality of subsequent steps. The vegetative amoebae needs to be broken by shear stress with a "steel ball cell cracker" (Balch, 1985), a method that preserves the integrity of subcellular organelles and in particular that of lysosomes, the rupture of which is very deleterious to further purifications. Subsequently, vesicles are isolated magnetically, especially lysosomes. Eventual crucial binding factors needed for Kif3's cargo selection and binding are still unknown. Taken together, a positive outcome of the experiment would have been doubtful.

An approach to the identification of Kif3's potential cellular function was the interruption of its gene by homologous recombination. Two independent constructs were used but both failed to establish a Kif3 knockout cell line. A possible explanation for the failure of the well-established method is that the structure of the *kif3* gene locus made a homologous recombination impossible. An alternative explanation lies in a possible lethality of Kif3-null cells. As described earlier, Unc104 and Kif3 may be redundant for vesicle transport, but there might also be a (yet unknown) cargo of Kif3 other than vesicles, crucial for *D. discoideum*'s survival. Although an antibody staining excluded an association of Kif3 with mitochondria during the vegetative stages of *D. discoideum*, it did not exclude an association during other cell stages, e.g. the mitosis. An incomplete distribution of mitochondria during cell division would most certainly result in lethality of at least the daughter cell. Taking a look at the method of *D. discoideum* transformation (2.3.16.2) reveals that single cells cannot be identified and selected for if they are not capable of producing survivable offspring.

A Western blot revealed a similar expression level of Kif3 throughout the entire lifecycle of *D. discoideum* cells. Nevertheless, it would be valuable to test this observation with real time PCR.

4.1.3 Conclusions

Kif3 is a processive kinesin that is more closely related to Nkin than to animal kinesin not only from the phylogenetic point of view, but also from its biochemical properties. The study focused mainly on the motor properties of Kif3, and therefore disregarded the functional properties of the tail domain. In evolution, however, the tail is likely to stand under tight selective pressure because it has been shown to connect to cellular cargo, and to regulate motor activity (Adio et al., 2006b). The unusual salt-dependence of Kif3 may indicate that this motor contains different or additional ways of regulation that can be induced by changes of the ionic strength. On the other hand, there is also considerable sequence similarity between fungal kinesins that are not as salt-sensitive as Kif3 in the tail domain, and future studies may show how these structural similarities are reflected in functional similarities.

Speculating about the evolution of conventional kinesins it seems that from the point of the animal fungal split the animal conventional kinesins lost their fast velocity, while fungal kinesins perpetuated the ancestral attributes comparable to those of *D. discoideum*.

4.2 *D. discoideum* Kif5

4.2.1 Biochemical properties

The purification of recombinant expressed Kif5-constructs always yielded Kif5 protein and additional contaminating proteins from *E. coli*. An exact determination of Kif5's concentration was therefore not possible, resulting in inaccurate values for the motor protein's biochemical analysis.

Nonetheless, ATPase and gliding assays were performed with Kif5-353 and Kif5-476, revealing a low microtubule activated ATPase activity. In gliding assays Kif5-476 was able to bind microtubules, but the velocity was below the detection limit. A substitution of ATP with AMP-PNP showed an increase in microtubule binding, indicating that the motor protein is functionally active but displays no (measurable) velocity. In the same experiment microtubule-binding of Kif5-353 could not be observed, indicating that due to its short structure - like Kif3-342 - the protein was not able to bind to the surface of the coverslip. Its microtubule induced ATPase activity is a strong argument against a functional defect.

4.2.2 Cellular localization and function of Kif5

The N-terminal GFP-fusion protein, comprising the full-length *kif5* gene, showed a distribution throughout the cell, but specifically enriched in the cell's cortex. A previous study demonstrated that the C-terminal tail of Kif5 directly interacts with actin filaments and that it bundles them *in vitro*. The localization of Kif5 at the actin-rich cell surface protrusions such as pseudopodia and crowns and its weak background staining throughout the cytoplasm lead to the theory of Kif5 being an organizer of the cytoskeleton in the highly motile cells of *D. discoideum* by bundling actin-filaments and connecting them to microtubules (Iwai et al., 2004). The fact that microtubule reassembly after nocodazole treatment was not affected in the knock out mutant excludes Kif5 from being an important organizer of the microtubule network during its establishment. Kif5-null cells showed no morphological or time variations in reorganizing their microtubules, leaving a possible organizing function only for moving cells. Due to the fast recovery of the microtubule arrays in less than 10 minutes and the fact that microtubules could only be stained with an antibody on fixed cells, a comparative study of chemotacting wild type and Kif5-null cells could not be performed.

A phenotype for the knockout of the *kif5* gene could not be detected during the microtubule re-organization and Kif5-null cells also did not reveal an apparent characteristic in any of the other experiments. The only discrepancy between wild type and null-mutant cells was observed in the growth rate of submerged cultures, but could not be discovered in shaking cultures. Apparently growth is only affected at more naturally related conditions. This observation indicates a slower progression of cell

division or even a defect in cell-surface adhesion, which plays an important role during cytokinesis. Studies on myosin II in *D. discoideum* revealed two mechanisms of cytokinesis: 1) cytokinesis with active furrowing under circumstances where cells cannot adhere to surfaces and 2) cell division resulting from traction forces generated by polar pseudopods exerting force on an adhesive surface (Zang et al., 1997). During cytokinesis, actin has been found in the furrow region by immunofluorescence (Fukui et al., 1990) and works in concert with myosin to form an active contractile ring to constrict the furrow and cleave the cell. Kif5 as a proposed actin-filament bundling protein (Iwai et al., 2004) has clearly no effect on the contractile ring formation, because then a disruption of the *kif5* gene would inevitably result in a reduced ability to cleave and separate the cell under non-adhering conditions. It is more likely that Kif5 acts on the formation of pseudopods and thereby limiting the speed of cytokinesis on adhesive surfaces.

In a previous study Kif5-null cells showed normal morphology at the vegetative stage and grew normally in an axenic suspension culture. Furthermore, they showed normal pinocytosis, phagocytosis, exocytosis, and contractile vacuole functions under hypo-osmotic conditions, and cell-cell adhesions. In the course of development upon starvation, the Kif5-null cells aggregated normally and formed fruiting bodies comparable with those of wild type cells (Iwai et al., 2004).

4.2.3 Conclusions

Kif5 shows a high degree of similarity of the motor domain with other members of conventional kinesins, sharing 53 % identity with *N. crassa*'s Nkin (Steinberg and Schliwa, 1995) and 52 % identity with human kinesin heavy chain (Navone et al., 1992). The close structural similarity to other conventional kinesins cannot be transferred to Kif5's biochemical properties. Although the conserved motor domain indicates a processive motor protein, biochemical assays revealed an almost non-functional kinesin with a low ATPase and no gliding activity. The suggested role as a cytoskeleton organizer makes a processive gliding activity dispensable and even a low ATPase activity is sufficient for sporadic microtubule binding events. The disruption of the *kif5*-gene revealed no apparent phenotype and leads to the assumption that Kif5 is not essential for the normal growth and development of *D. discoideum* cells under laboratory conditions. However, an involvement of Kif5 on cytokinesis under adhesive conditions needs to be further investigated.

The most intriguing fact of Kif5 is its close relationship to the conventional kinesins. It seems that *D. discoideum* used the product of a kinesin gene duplication to organize its cytoskeleton during movement. This theory would explain why *D. discoideum*, of all other compared organisms except mammals, contains more than one conventional kinesin (Kollmar and Glockner, 2003).

5 References

- Adio, S., Bloemink, M., Hartel, M., Leier, S., Geeves, M. A. and Woehlke, G.** (2006a). Kinetic and mechanistic basis of the nonprocessive Kinesin-3 motor NcKin3. *J Biol Chem* **281**, 37782-93.
- Adio, S., Reth, J., Bathe, F. and Woehlke, G.** (2006b). Review: regulation mechanisms of Kinesin-1. *J Muscle Res Cell Motil* **27**, 153-60.
- Alivisatos, A. P., Gu, W. and Larabell, C.** (2005). Quantum dots as cellular probes. *Annu Rev Biomed Eng* **7**, 55-76.
- Andrews, P.** (1970). Estimation of molecular size and molecular weights of biological compounds by gel filtration. *Methods Biochem Anal* **18**, 1-53.
- Asbury, C. L.** (2005). Kinesin: world's tiniest biped. *Curr Opin Cell Biol* **17**, 89-97.
- Asbury, C. L., Fehr, A. N. and Block, S. M.** (2003). Kinesin moves by an asymmetric hand-over-hand mechanism. *Science* **302**, 2130-4.
- Aubry, L. K., G.** (2006). Purification Techniques of Subcellular Compartments for Analytical and Preparative Purposes. *Methods in Molecular Biology* **346**, 171-185.
- Auerbach, S. D. and Johnson, K. A.** (2005). Alternating site ATPase pathway of rat conventional kinesin. *J Biol Chem* **280**, 37048-60.
- Balch, W. E. R., J.E.** (1985). Characterization of Protein Transport between successive Compartments of the Golgi Apparatus: Asymmetric Properties of Donor and Acceptor activities in a Cell-free system. *Arch Biochem Biophys* **240**, 413-425.
- Bohm, K. J., Stracke, R., Baum, M., Zieren, M. and Unger, E.** (2000). Effect of temperature on kinesin-driven microtubule gliding and kinesin ATPase activity. *FEBS Lett* **466**, 59-62.
- Brady, S. T.** (1985). A novel brain ATPase with properties expected for the fast axonal transport motor. *Nature* **317**, 73-5.
- Brady, S. T., Lasek, R. J. and Allen, R. D.** (1985). Video microscopy of fast axonal transport in extruded axoplasm: a new model for study of molecular mechanisms. *Cell Motil* **5**, 81-101.
- Cai, D., Verhey, K. J. and Meyhofer, E.** (2007). Tracking single Kinesin molecules in the cytoplasm of mammalian cells. *Biophys J* **92**, 4137-44.
- Cantor, C. R. S., P. R.** (1980). Techniques for the Study of Biological Structure and Function. San Francisco: W. H. Freeman.
- Carter, N. J. and Cross, R. A.** (2005). Mechanics of the kinesin step. *Nature* **435**, 308-12.
- Claviez, M., Pagh, K., Maruta, H., Baltes, W., Fisher, P. and Gerisch, G.** (1982). Electron microscopic mapping of monoclonal antibodies on the tail region of Dictyostelium myosin. *Embo J* **1**, 1017-1022.
- Coy, D. L., Hancock, W. O., Wagenbach, M. and Howard, J.** (1999). Kinesin's tail domain is an inhibitory regulator of the motor domain. *Nat Cell Biol* **1**, 288-92.
- Dagenbach, E. M. and Endow, S. A.** (2004). A new kinesin tree. *J Cell Sci* **117**, 3-7.

- Daunderer, C. and Graf, R. O.** (2002). Molecular analysis of the cytosolic Dictyostelium gamma-tubulin complex. *Eur J Cell Biol* **81**, 175-84.
- de Hostos, E. L., McCaffrey, G., Sugang, R., Pierce, D. W. and Vale, R. D.** (1998). A developmentally regulated kinesin-related motor protein from Dictyostelium discoideum. *Mol Biol Cell* **9**, 2093-106.
- Eichinger, L.** (2003). Revamp a model-status and prospects of the Dictyostelium genome project. *Curr Genet* **44**, 59-72.
- Eichinger, L. and Noegel, A. A.** (2005). Comparative genomics of Dictyostelium discoideum and Entamoeba histolytica. *Curr Opin Microbiol* **8**, 606-11.
- Eichinger, L., Pachebat, J. A., Glockner, G., Rajandream, M. A., Sugang, R., Berriman, M., Song, J., Olsen, R., Szafranski, K., Xu, Q., Tunggal, B., Kummerfeld, S., Madera, M., Konfortov, B. A., Rivero, F., Bankier, A. T., Lehmann, R., Hamlin, N., Davies, R., Gaudet, P., Fey, P., Pilcher, K., Chen, G., Saunders, D., Sodergren, E., Davis, P., Kerhornou, A., Nie, X., Hall, N., Anjard, C., Hemphill, L., Bason, N., Farbrother, P., Desany, B., Just, E., Morio, T., Rost, R., Churcher, C., Cooper, J., Haydock, S., van Driessche, N., Cronin, A., Goodhead, I., Muzny, D., Mourier, T., Pain, A., Lu, M., Harper, D., Lindsay, R., Hauser, H., James, K., Quiles, M., Madan Babu, M., Saito, T., Buchrieser, C., Wardroper, A., Felder, M., Thangavelu, M., Johnson, D., Knights, A., Louseged, H., Mungall, K., Oliver, K., Price, C., Quail, M. A., Urushihara, H., Hernandez, J., Rabinowitsch, E., Steffen, D., Sanders, M., Ma, J., Kohara, Y., Sharp, S., Simmonds, M., Spiegler, S., Tivey, A., Sugano, S., White, B., Walker, D., Woodward, J., Winckler, T., Tanaka, Y., Shaulsky, G., Schleicher, M., Weinstock, G., Rosenthal, A., Cox, E. C., Chisholm, R. L., Gibbs, R., Loomis, W. F., Platzer, M., Kay, R. R., Williams, J., Dear, P. H., Noegel, A. A., Barrell, B. and Kuspa, A.** (2005). The genome of the social amoeba Dictyostelium discoideum. *Nature* **435**, 43-57.
- Faix, J., Kreppel, L., Shaulsky, G., Schleicher, M. and Kimmel, A. R.** (2004). A rapid and efficient method to generate multiple gene disruptions in Dictyostelium discoideum using a single selectable marker and the Cre-loxP system. *Nucleic Acids Res* **32**, e143.
- Faix, J., Weber, I., Mintert, U., Kohler, J., Lottspeich, F. and Marriott, G.** (2001). Recruitment of cortexillin into the cleavage furrow is controlled by Rac1 and IQGAP-related proteins. *Embo J* **20**, 3705-15.
- Fersht, A.** (1999). Structure and Mechanism in Protein Science. Guide to Enzyme Catalysis and Protein Folding. Hampshire, UK: Palgrave Macmillan.
- Fischer, M., Haase, I., Simmeth, E., Gerisch, G. and Muller-Taubenberger, A.** (2004). A brilliant monomeric red fluorescent protein to visualize cytoskeleton dynamics in Dictyostelium. *FEBS Lett* **577**, 227-32.
- Fortunato, A., Strassmann, J. E., Santorelli, L. and Queller, D. C.** (2003). Co-occurrence in nature of different clones of the social amoeba, Dictyostelium discoideum. *Mol Ecol* **12**, 1031-8.
- Fuchs, F. and Westermann, B.** (2005). Role of Unc104/KIF1-related motor proteins in mitochondrial transport in Neurospora crassa. *Mol Biol Cell* **16**, 153-61.

- Fukui, Y., De Lozanne, A. and Spudich, J. A.** (1990). Structure and function of the cytoskeleton of a Dictyostelium myosin-defective mutant. *J Cell Biol* **110**, 367-78.
- Goldstein, L. S.** (2001). Molecular motors: from one motor many tails to one motor many tales. *Trends Cell Biol* **11**, 477-82.
- Graf, R., Euteneuer, U., Ho, T. H. and Rehberg, M.** (2003). Regulated expression of the centrosomal protein DdCP224 affects microtubule dynamics and reveals mechanisms for the control of supernumerary centrosome number. *Mol Biol Cell* **14**, 4067-74.
- Grummt, M., Pistor, S., Lottspeich, F. and Schliwa, M.** (1998). Cloning and functional expression of a 'fast' fungal kinesin. *FEBS Lett* **427**, 79-84.
- Guex, N. and Peitsch, M. C.** (1997). SWISS-MODEL and the Swiss-PdbViewer: an environment for comparative protein modeling. *Electrophoresis* **18**, 2714-23.
- Hackney, D. D.** (1994). The rate-limiting step in microtubule-stimulated ATP hydrolysis by dimeric kinesin head domains occurs while bound to the microtubule. *J Biol Chem* **269**, 16508-11.
- Hackney, D. D.** (1995). Implications of diffusion-controlled limit for processivity of dimeric kinesin head domains. *Biophys J* **68**, 267S-269S; discussion 269S-270S.
- Hackney, D. D.** (2005). The tethered motor domain of a kinesin-microtubule complex catalyzes reversible synthesis of bound ATP. *Proc Natl Acad Sci U S A* **102**, 18338-43.
- Hackney, D. D., Levitt, J. D. and Suhan, J.** (1992). Kinesin undergoes a 9 S to 6 S conformational transition. *J Biol Chem* **267**, 8696-701.
- Hackney, D. D. and Stock, M. F.** (2000). Kinesin's IAK tail domain inhibits initial microtubule-stimulated ADP release. *Nat Cell Biol* **2**, 257-60.
- Hagedorn, M., Neuhaus, E. M. and Soldati, T.** (2006). Optimized fixation and immunofluorescence staining methods for Dictyostelium cells. *Methods Mol Biol* **346**, 327-38.
- Hancock, W. O. and Howard, J.** (1998). Processivity of the motor protein kinesin requires two heads. *J Cell Biol* **140**, 1395-405.
- Hestermann, A. and Graf, R.** (2004). The XMAP215-family protein DdCP224 is required for cortical interactions of microtubules. *BMC Cell Biol* **5**, 24.
- Hirokawa, N.** (1998). Kinesin and dynein superfamily proteins and the mechanism of organelle transport. *Science* **279**, 519-26.
- Hirokawa, N., Noda, Y. and Okada, Y.** (1998). Kinesin and dynein superfamily proteins in organelle transport and cell division. *Curr Opin Cell Biol* **10**, 60-73.
- Hirokawa, N., Pfister, K. K., Yorifuji, H., Wagner, M. C., Brady, S. T. and Bloom, G. S.** (1989). Submolecular domains of bovine brain kinesin identified by electron microscopy and monoclonal antibody decoration. *Cell* **56**, 867-78.
- Howard, J.** (2001). *Mechanics of Motor Proteins and the Cytoskeleton*. Sunderland, Massachusetts: Sinauer Associates, Inc.
- Inoue, H., Nojima, H. and Okayama, H.** (1990). High efficiency transformation of Escherichia coli with plasmids. *Gene* **96**, 23-8.

- Iwai, S., Ishiji, A., Mabuchi, I. and Sutoh, K. (2004). A novel actin-bundling kinesin-related protein from *Dictyostelium discoideum*. *J Biol Chem* **279**, 4696-704.
- Jeong, J. W., Rhee, D. K., Cho, S. Y., Hae, K. L., Kim, D. U., Won, M. and Kim, H. B. (2002). Cloning and characterization of the kinesin-related protein, Krp1p, in *Schizosaccharomyces pombe*. *Mol Cells* **13**, 389-98.
- Jiang, M. Y. and Sheetz, M. P. (1995). Cargo-activated ATPase activity of kinesin. *Biophys J* **68**, 283S-284S; discussion 285S.
- Jiang, W. and Hackney, D. D. (1997). Monomeric kinesin head domains hydrolyze multiple ATP molecules before release from a microtubule. *J Biol Chem* **272**, 5616-21.
- Kallipolitou, A., Deluca, D., Majdic, U., Lakamper, S., Cross, R., Meyhofer, E., Moroder, L., Schliwa, M. and Woehlke, G. (2001). Unusual properties of the fungal conventional kinesin neck domain from *Neurospora crassa*. *Embo J* **20**, 6226-35.
- Kaseda, K., Higuchi, H. and Hirose, K. (2003). Alternate fast and slow stepping of a heterodimeric kinesin molecule. *Nat Cell Biol* **5**, 1079-82.
- Khodjakov, A., Lizunova, E. M., Minin, A. A., Koonce, M. P. and Gyoeva, F. K. (1998). A specific light chain of kinesin associates with mitochondria in cultured cells. *Mol Biol Cell* **9**, 333-43.
- Kimble, M., Kuzmiak, C., McGovern, K. N. and de Hostos, E. L. (2000). Microtubule organization and the effects of GFP-tubulin expression in *dictyostelium discoideum*. *Cell Motil Cytoskeleton* **47**, 48-62.
- Kirchner, J., Woehlke, G. and Schliwa, M. (1999). Universal and unique features of kinesin motors: insights from a comparison of fungal and animal conventional kinesins. *Biol Chem* **380**, 915-21.
- Klopfenstein, D. R., Holleran, E. A. and Vale, R. D. (2002). Kinesin motors and microtubule-based organelle transport in *Dictyostelium discoideum*. *J Muscle Res Cell Motil* **23**, 631-8.
- Kollmar, M. and Glockner, G. (2003). Identification and phylogenetic analysis of *Dictyostelium discoideum* kinesin proteins. *BMC Genomics* **4**, 47.
- Koonce, M. P. and Khodjakov, A. (2002). Dynamic microtubules in *Dictyostelium*. *J Muscle Res Cell Motil* **23**, 613-9.
- Kozielski, F., Sack, S., Marx, A., Thormahlen, M., Schonbrunn, E., Biou, V., Thompson, A., Mandelkow, E. M. and Mandelkow, E. (1997). The crystal structure of dimeric kinesin and implications for microtubule-dependent motility. *Cell* **91**, 985-94.
- Kyhse-Anderson, J. (1984). Electrophoretic transfer of multiple gels: a simple apparatus without buffer tank for rapid transfer of proteins from polyacrylamide to nitrocellulose. *J. Biochem. Biophys. Meth.* **10**, 203-209.
- Lawrence, C. J., Dawe, R. K., Christie, K. R., Cleveland, D. W., Dawson, S. C., Endow, S. A., Goldstein, L. S., Goodson, H. V., Hirokawa, N., Howard, J., Malmberg, R. L., McIntosh, J. R., Miki, H., Mitchison, T. J., Okada, Y., Reddy, A. S., Saxton, W. M., Schliwa, M., Scholey, J. M., Vale, R. D., Walczak, C. E. and Wordeman, L. (2004). A standardized kinesin nomenclature. *J Cell Biol* **167**, 19-22.

- Ma, S., Fey, P. and Chisholm, R. L.** (2001). Molecular motors and membrane traffic in Dictyostelium. *Biochim Biophys Acta* **1525**, 234-44.
- Ma, Y. Z. and Taylor, E. W.** (1997). Interacting head mechanism of microtubule-kinesin ATPase. *J Biol Chem* **272**, 724-30.
- Malchow, D., Nagele, B., Schwarz, H. and Gerisch, G.** (1972). Membrane-bound cyclic AMP phosphodiesterase in chemotactically responding cells of Dictyostelium discoideum. *Eur J Biochem* **28**, 136-42.
- Malik, F., Brillinger, D. and Vale, R. D.** (1994). High-resolution tracking of microtubule motility driven by a single kinesin motor. *Proc Natl Acad Sci U S A* **91**, 4584-8.
- Mazumdar, M. and Cross, R. A.** (1998). Engineering a lever into the kinesin neck. *J Biol Chem* **273**, 29352-9.
- McIntosh, J. R., Roos, U. P., Neighbors, B. and McDonald, K. L.** (1985). Architecture of the microtubule component of mitotic spindles from Dictyostelium discoideum. *J Cell Sci* **75**, 93-129.
- Michalet, X., Pinaud, F. F., Bentolila, L. A., Tsay, J. M., Doose, S., Li, J. J., Sundaresan, G., Wu, A. M., Gambhir, S. S. and Weiss, S.** (2005). Quantum dots for live cells, in vivo imaging, and diagnostics. *Science* **307**, 538-44.
- Muller-Taubenberger, A., Lupas, A. N., Li, H., Ecke, M., Simmeth, E. and Gerisch, G.** (2001). Calreticulin and calnexin in the endoplasmic reticulum are important for phagocytosis. *Embo J* **20**, 6772-82.
- Nangaku, M., Sato-Yoshitake, R., Okada, Y., Noda, Y., Takemura, R., Yamazaki, H. and Hirokawa, N.** (1994). KIF1B, a novel microtubule plus end-directed monomeric motor protein for transport of mitochondria. *Cell* **79**, 1209-20.
- Navone, F., Niclas, J., Hom-Booher, N., Sparks, L., Bernstein, H. D., McCaffrey, G. and Vale, R. D.** (1992). Cloning and expression of a human kinesin heavy chain gene: interaction of the COOH-terminal domain with cytoplasmic microtubules in transfected CV-1 cells. *J Cell Biol* **117**, 1263-75.
- Pereira, A. J., Dalby, B., Stewart, R. J., Doxsey, S. J. and Goldstein, L. S.** (1997). Mitochondrial association of a plus end-directed microtubule motor expressed during mitosis in Drosophila. *J Cell Biol* **136**, 1081-90.
- Pollock, N., de Hostos, E. L., Turck, C. W. and Vale, R. D.** (1999). Reconstitution of membrane transport powered by a novel dimeric kinesin motor of the Unc104/KIF1A family purified from Dictyostelium. *J Cell Biol* **147**, 493-506.
- Raper, K. B.** (1935). Dictyostelium discoideum, a new species of slime mold from decaying forest leaves. *J. Agr. Res.*, 135-147.
- Ray, S., Meyhofer, E., Milligan, R. A. and Howard, J.** (1993). Kinesin follows the microtubule's protofilament axis. *J Cell Biol* **121**, 1083-93.
- Rehberg, M., Kleylein-Sohn, J., Faix, J., Ho, T. H., Schulz, I. and Graf, R.** (2005). Dictyostelium LIS1 is a centrosomal protein required for microtubule/cell cortex interactions, nucleus/centrosome linkage, and actin dynamics. *Mol Biol Cell* **16**, 2759-71.
- Rodriguez-Paris, J. M., Nolta, K. V. and Steck, T. L.** (1993). Characterization of lysosomes isolated from Dictyostelium discoideum by magnetic fractionation. *J Biol Chem* **268**, 9110-6.

- Ronquist, F. and Huelsenbeck, J. P. (2003). MrBayes 3: Bayesian phylogenetic inference under mixed models. *Bioinformatics* **19**, 1572-4.
- Roos, U. P. (1987). Probing the mechanisms of mitosis with Dictyostelium discoideum. *Methods Cell Biol* **28**, 261-79.
- Roos, U. P., De Brabander, M. and De Mey, J. (1984). Indirect immunofluorescence of microtubules in Dictyostelium discoideum. A study with polyclonal and monoclonal antibodies to tubulins. *Exp Cell Res* **151**, 183-93.
- Saitou, N. and Nei, M. (1987). The neighbor-joining method: a new method for reconstructing phylogenetic trees. *Mol Biol Evol* **4**, 406-25.
- Sambrook, J. F., E.F.; Maniatis. (1989). Molecular Cloning: A laboratory manual. New York: Cold Spring Harbor Laboratory Press.
- Schaap, P., Winckler, T., Nelson, M., Alvarez-Curto, E., Elgie, B., Hagiwara, H., Cavender, J., Milano-Curto, A., Rozen, D. E., Dingermann, T., Mutzel, R. and Baldauf, S. L. (2006). Molecular phylogeny and evolution of morphology in the social amoebas. *Science* **314**, 661-3.
- Schliwa, M. (1989). Head and tail. *Cell* **56**, 719-20.
- Schliwa, M. (2003). Kinesin: walking or limping? *Nat Cell Biol* **5**, 1043-4.
- Schwede, T., Kopp, J., Guex, N. and Peitsch, M. C. (2003). SWISS-MODEL: An automated protein homology-modeling server. *Nucleic Acids Res* **31**, 3381-5.
- Seiler, S., Kirchner, J., Horn, C., Kallipolitou, A., Woehlke, G. and Schliwa, M. (2000). Cargo binding and regulatory sites in the tail of fungal conventional kinesin. *Nat Cell Biol* **2**, 333-8.
- Seitz, A. and Surrey, T. (2006). Processive movement of single kinesins on crowded microtubules visualized using quantum dots. *Embo J* **25**, 267-77.
- Shimizu, T., Thorn, K. S., Ruby, A. and Vale, R. D. (2000). ATPase kinetic characterization and single molecule behavior of mutant human kinesin motors defective in microtubule-based motility. *Biochemistry* **39**, 5265-73.
- Soldati, T. and Schliwa, M. (2006). Powering membrane traffic in endocytosis and recycling. *Nat Rev Mol Cell Biol* **7**, 897-908.
- Sproul, L. R., Anderson, D. J., Mackey, A. T., Saunders, W. S. and Gilbert, S. P. (2005). Cik1 targets the minus-end kinesin depolymerase kar3 to microtubule plus ends. *Curr Biol* **15**, 1420-7.
- Steinberg, G. and Schliwa, M. (1995). The Neurospora organelle motor: a distant relative of conventional kinesin with unconventional properties. *Mol Biol Cell* **6**, 1605-18.
- Steinberg, G. and Schliwa, M. (1996). Characterization of the biophysical and motility properties of kinesin from the fungus Neurospora crassa. *J Biol Chem* **271**, 7516-21.
- Stock, M. F., Chu, J. and Hackney, D. D. (2003). The kinesin family member BimC contains a second microtubule binding region attached to the N terminus of the motor domain. *J Biol Chem* **278**, 52315-22.
- Studier, F. W., Rosenberg, A. H., Dunn, J. J. and Dubendorff, J. W. (1990). Use of T7 RNA polymerase to direct expression of cloned genes. *Methods Enzymol* **185**, 60-89.

- Svoboda, K., Mitra, P. P. and Block, S. M.** (1994). Fluctuation analysis of motor protein movement and single enzyme kinetics. *Proc Natl Acad Sci U S A* **91**, 11782-6.
- Tanaka, Y., Kanai, Y., Okada, Y., Nonaka, S., Takeda, S., Harada, A. and Hirokawa, N.** (1998). Targeted disruption of mouse conventional kinesin heavy chain, kif5B, results in abnormal perinuclear clustering of mitochondria. *Cell* **93**, 1147-58.
- Thompson, J. D., Gibson, T. J., Plewniak, F., Jeanmougin, F. and Higgins, D. G.** (1997). The CLUSTAL_X windows interface: flexible strategies for multiple sequence alignment aided by quality analysis tools. *Nucleic Acids Res* **25**, 4876-82.
- Thompson, J. D., Thierry, J. C. and Poch, O.** (2003). RASCAL: rapid scanning and correction of multiple sequence alignments. *Bioinformatics* **19**, 1155-61.
- Troll, H., Malchow, D., Muller-Taubenberger, A., Humbel, B., Lottspeich, F., Ecke, M., Gerisch, G., Schmid, A. and Benz, R.** (1992). Purification, functional characterization, and cDNA sequencing of mitochondrial porin from *Dictyostelium discoideum*. *J Biol Chem* **267**, 21072-9.
- Ueda, M., Schliwa, M. and Euteneuer, U.** (1999). Unusual centrosome cycle in *Dictyostelium*: correlation of dynamic behavior and structural changes. *Mol Biol Cell* **10**, 151-60.
- Uemura, S., Kawaguchi, K., Yajima, J., Edamatsu, M., Toyoshima, Y. Y. and Ishiwata, S.** (2002). Kinesin-microtubule binding depends on both nucleotide state and loading direction. *Proc Natl Acad Sci U S A* **99**, 5977-81.
- Vale, R. D.** (1996). Switches, latches, and amplifiers: common themes of G proteins and molecular motors. *J Cell Biol* **135**, 291-302.
- Vale, R. D., Reese, T. S. and Sheetz, M. P.** (1985a). Identification of a novel force-generating protein, kinesin, involved in microtubule-based motility. *Cell* **42**, 39-50.
- Vale, R. D., Schnapp, B. J., Mitchison, T., Steuer, E., Reese, T. S. and Sheetz, M. P.** (1985b). Different axoplasmic proteins generate movement in opposite directions along microtubules in vitro. *Cell* **43**, 623-32.
- Valentine, M. T. and Gilbert, S. P.** (2007). To step or not to step? How biochemistry and mechanics influence processivity in Kinesin and Eg5. *Curr Opin Cell Biol* **19**, 75-81.
- Wedlich-Soldner, R., Straube, A., Friedrich, M. W. and Steinberg, G.** (2002). A balance of KIF1A-like kinesin and dynein organizes early endosomes in the fungus *Ustilago maydis*. *Embo J* **21**, 2946-57.
- Westphal, M., Jungbluth, A., Heidecker, M., Muhlbauer, B., Heizer, C., Schwartz, J. M., Marriott, G. and Gerisch, G.** (1997). Microfilament dynamics during cell movement and chemotaxis monitored using a GFP-actin fusion protein. *Curr Biol* **7**, 176-83.
- Wickstead, B. and Gull, K.** (2006). A "holistic" kinesin phylogeny reveals new kinesin families and predicts protein functions. *Mol Biol Cell* **17**, 1734-43.
- Woehlke, G., Ruby, A. K., Hart, C. L., Ly, B., Hom-Booher, N. and Vale, R. D.** (1997). Microtubule interaction site of the kinesin motor. *Cell* **90**, 207-16.

- Woehlke, G. and Schliwa, M.** (2000). Walking on two heads: the many talents of kinesin. *Nat Rev Mol Cell Biol* **1**, 50-8.
- Yildiz, A. and Selvin, P. R.** (2005). Kinesin: walking, crawling or sliding along? *Trends Cell Biol* **15**, 112-20.
- Yildiz, A., Tomishige, M., Vale, R. D. and Selvin, P. R.** (2004). Kinesin walks hand-over-hand. *Science* **303**, 676-8.
- Yonekura, H., Nomura, A., Ozawa, H., Tatsu, Y., Yumoto, N. and Uyeda, T. Q.** (2006). Mechanism of tail-mediated inhibition of kinesin activities studied using synthetic peptides. *Biochem Biophys Res Commun* **343**, 420-7.
- Zang, J. H., Cavet, G., Sabry, J. H., Wagner, P., Moores, S. L. and Spudich, J. A.** (1997). On the role of myosin-II in cytokinesis: division of Dictyostelium cells under adhesive and nonadhesive conditions. *Mol Biol Cell* **8**, 2617-29.

Acknowledgments

Ich möchte mich ganz herzlich bei allen Mitgliedern der Arbeitsgruppen von Prof. Schliwa und Prof. Schleicher für die freundliche Aufnahme und Einführung in den Münchner Laborarbeitsalltag bedanken. Die „Kränzchen“ und dienstags Arbeitsgruppen meetings haben mich häufig zu neuen Ideen und Lösungsansätzen inspiriert. Bei Problemen oder bei neuen Versuchen gab es stets Ansprechpartner in beiden Gruppen, die sich kompetent und schnell um meine Belange gekümmert haben.

Im Einzelnen danken möchte ich...

PD Dr. Günther Woehlke für die Betreuung und Beratung bei der Durchführung wissenschaftlicher Arbeiten und beim Schreiben der Publikation und dieser Arbeit. Probleme mit modernen Arbeitsgeräten und ihrer Software konnten durch seine Hilfe zügig und nachhaltig beseitigt werden.

Prof. Dr. Manfred Schliwa für die Aufnahme in das Institut für Zellbiologie und somit zur Ermöglichung dieser Arbeit.

Dr. Irene Schulz und Prof. Dr. Ralph Gräf, die insbesondere am Anfang der Dissertation viel Zeit und Geduld investiert haben, um mir *Dicty* und seine manchmal merkwürdig anmutenden Eigenschaften nahe zu bringen.

Sven Leier und Thi-Hieu Ho. Ohne deren Fleiß und Verlässlichkeit wären viele Arbeitsabläufe und Versuche deutlich langsamer und vielleicht auch nicht ganz so erfolgreich verlaufen.

Bettina Ebbing für die Einführung in das TIRF Mikroskop und allen damit verbundenen Versuchsaufbauten.

Dr. Zeynep Ökten und Dr. Meino Rohlf für die sprachliche und inhaltliche Durchsicht dieser Arbeit.

Allen ehemaligen und aktuellen Mitgliedern des Mittagsstammtisches, die das Essen in der Mensa erträglich gemacht haben und stets für gute Laune sorgten.

Meinen Eltern gebührt besonderer Dank. Ohne ihre Unterstützung, sowohl moralisch, als auch finanziell, wären weder das Studium, noch diese Dissertation möglich gewesen. Besonders bedanken möchte ich mich auch bei meiner Freundin und Lebensgefährtin Dr. Kathrin Söffge, die stets an ein positives Ende der Dissertation geglaubt hat und auch bei Fehlschlägen oder anderen schwierigen Situationen zu mir gehalten hat.

Curriculum vitae

Name Christian Röhlk
Date of birth Apr 13, 1977
Place of birth Göttingen, Germany

Academic Education

01/2007-06/2007 Change of lab with Dr. G. Woehlke to the Dept. of Physics E22, Technical University Munich
12/2006 Poster presentation at the Congress of the American Society of Cell Biology in San Diego, CA, USA
10/2003-12/2006 PhD thesis in the group of Dr. G. Woehlke (Abt. Prof. M. Schliwa) at the Institute for Cell Biology, Ludwig-Maximilians-University, Munich
11/2002-09/2003 Diploma thesis „Analyse der Mechanismen der epithelialen Abwehr in *Hydra*“ at the lab of Prof. Dr. T. Bosch, Kiel
10/1998-09/2003 Study of Biology at the Christian-Albrechts-Universität zu Kiel

09/1997-06/1998 Military service

School education

06/1997 General qualification for university entrance (Abitur)
1994-1997 Gymnasium Brunsbüttel
1993-1994 Nacogdoches High School, Nacogdoches, TX, USA
1987-1993 Gymnasium Brunsbüttel
1983-1987 Primary School Burg in Dithmarschen (Schleswig-Holstein)